https://doi.org/10.5194/gchron-2019-18
Preprint. Discussion started: 20 January 2020

Seasonal deposition processes and chronology of a varved Holocene lake sediment record from Lake Chatyr Kol (Kyrgyz Republic)

Julia Kalanke[1], Jens Mingram[1], Stefan Lauterbach[2], Ryskul Usubaliev[3], Achim Brauer[1,4]

[1]GFZ German Research Centre for Geosciences, Section 'Climate Dynamics and Landscape Evolution', Potsdam, Germany
[2]University of Kiel, Leibniz Laboratory for Radiometric Dating and Stable Isotope Research, Kiel, Germany
[3]Central Asian Institute for Applied Geoscience, Bishkek, Kyrgyzstan
[4]University of Potsdam, Institute of Geoscience, Potsdam, Germany

Correspondence to: Julia Kalanke (juliak@gfz-potsdam.de)
Telegrafenberg C322
14473 Potsdam/Germany
+49 331 288-1379

Abstract.

A finely laminated lake sediment record with a basal age of 11,619 ± 603 years BP was retrieved from Lake Chatyr Kol (Kyrgyz Republic). Microfacies analysis reveals the presence of seasonal laminae (varves) from the sediment basis to ~360 ± 40 years BP. The Chatvd19 floating varve chronology covers the time span from 360 ± 40 years BP to the base and relies on replicate varve counts on overlapping petrographic thin sections with an uncertainty of ± 5 %. The uppermost non-varved interval was chronologically constrained by ^{210}Pb and ^{137}Cs γ-spectrometry and interpolation based on varve thickness measurements of adjacent varved intervals with an assumed uncertainty of 10 %. Six varve types were distinguished, are described in detail and show a changing predominance of clastic-organic, clastic-calcitic or -aragonitic, calcitic-clastic, organic-clastic and clastic-diatom varves throughout the Holocene. Variations in varve thickness and the number and composition of seasonal sublayers are attributed to 1) changes in the amount of summer or winter/spring precipitation affecting local runoff and erosion and/or to 2) evaporative conditions during summer. Radiocarbon dating of bulk organic matter, daphnia remains, aquatic plant remains and *Ruppia maritima* seeds reveal reservoir ages with a clear decreasing trend up core from ~6,150 years in the early Holocene, to ~3,000 years in the mid-Holocene, to ~1,000 years and less in the late Holocene and modern times. In contrast, two radiocarbon dates from terrestrial plant remains are in good agreement with the varve-based chronology.

https://doi.org/10.5194/gchron-2019-18
Preprint. Discussion started: 20 January 2020

1 Introduction

The interplay of the large atmospheric circulation systems in Central Asia (CA), including the Siberian High, the Westerlies and the Indian Monsoon and their influences on regional climate is still not fully understood. This is partly due to the large contrasts of landscapes (high mountains, deep basins, large water bodies and deserts), the low spatial and temporal coverage of high-resolution paleo-climate archives and the partly problematic dating of these archives in this area. Information about Holocene climate variability in CA derive from several types of archives, including tree rings (Esper et al., 2003; Raspopov et al., 2008), speleothems (Fohlmeister et al., 2017; Wolff et al., 2017), ice cores (Aizen, 2004), aeolian deposits (Huayu et al., 2010) and lakes (Heinecke et al., 2017; Lauterbach et al., 2014; Mathis et al., 2014; Rasmussen et al., 2000; Ricketts et al., 2001; Schwarz et al., 2017). However, none of these lake records has reported annually laminated sediments. The nearest varved lake sediment records are reported from Lake Sary Chelek (Kyrgyzstan) where varved sediments cover only the most recent times from ~1940´s to 2013 (Lauterbach et al., 2019), from Lake Telmen in northern Mongolia which cover approximately 7,100 cal years BP (Peck, 2002) and from Lake Sugan in north western China covering ~2,700 years BP (Zhou et al., 2007). Deciphering Holocene climate changes based on limnic records in CA is challenging due to the influences of several factors: 1) chronological uncertainties caused by the scarcity of datable terrestrial plant material at high altitudes and often large 14C reservoir effects of aquatic organic material (Hou et al., 2012; Lockot et al., 2016; Mischke et al., 2013), 2) human influence n(Boomer et al., 2000; Mathis et al., 2014; Schröter et al., 2019 in review), possibly overprinting the natural climate signals in the archives and 3) variations in the dominance of the mid-latitude Westerlies, the Siberian High and the Asian Monsoon system leading to different spatial and temporal climate effects over CA (Chen et al., 2008; Herzschuh, 2006; Mischke et al., 2017). All these factors can hamper data comparison and may lead to different paleo-environmental interpretations (Chen et al., 2008; Hou et al., 2012; Mischke et al., 2017). The investigation of varved lake sediments offers the unique opportunity for independent dating through varve counting. In addition, varve micro-facies provides detailed insights into environmental and climate variations at a seasonal scale. Variations in the depositional regime are largely controlled by climate conditions and thus potentially linked to atmospheric circulation regimes. The sediment record from Lake Chatyr Kol is the first varved record from CA covering most of the Holocene and, therefore, was investigated within the framework of the projects CADY (Central Asian Climate Dynamics) and CAHOL (Central Asian Holocene Climate) to gain a more detailed understanding of Holocene climate changes in this region.

This study focusses on 1) sediment microfacies analysis to identify Holocene seasonal deposition patterns, a prerequisite for the proof of varves, and, 2) the development of a robust age model based on varve counting to determine the time of changes within the ecosystem.

https://doi.org/10.5194/gchron-2019-18
Preprint. Discussion started: 20 January 2020

2. Study site

Lake Chatyr Kol (40°36' N, 75°14' E) (Fig.1) is located at ~3,530 m above sea level (a.s.l.) in the intramontane Aksai Basin (De Grave et al., 2011; Koppes et al., 2008) in the southern Kyrgyz Republic. In the north, the basin is restricted by the At Bashy Range and in the south by the Torugat Range resulting in a catchment area of about 1084 km2. Geologically, the surrounding mountain ranges belong to Silurian – to Carboniferous sedimentary-volcanogenic complexes of marine-continental collision zones, consisting of limestones and dolomites, that crop out directly along the northern lake shore, as well as siliceous rocks, shales and scattered Permian granites that crop out in the south and north-east (Academy of Science of the Kyrgyz SSR, 1987). The modern lake, which has a maximum length of 23 km, a width of 10 km and a maximum depth of 20 m in its western-central part, is endorheic and separated from the neighboring Arpa river basin in the north-west by a moraine (Shnitnikov, 1978) while a shallow watershed hinders outflow to the east. The lake is mainly fed by the small Kegagyr River in the east, by meltwater runoff and convective rainfall events in summer (Aizen et al., 2001). Modern climate conditions are generally dry and mainly controlled by the Westerlies and the Siberian Anticyclone Circulation (Aizen et al., 2001; Koppes et al., 2008). Mean annual precipitation is ~275 mm/a as indicated by Aizen´s (2001) evaluation and spatial averaging of annual precipitation amounts of historical records published by Hydrometeo (Reference Book of Climate USSR, Kyrgyz SSR, 1988). This is comparable to long-term instrumental data from nearby (about 50 km away) weather stations at comparable altitudes, where annual precipitation means are 237 mm/a (station "Chatirkul", 75°8´E, 40°6´N, 3,540 m a.s.l, AD 1961–1990) and 294 mm/a (station "TienShan", 78°2´E, 41°9´N, 3,614 m a.s.l., AD 1930–2000) (Williams and Konovalov, 2008). Monthly mean temperatures range from -26.0 to 8.0 °C (Koppes et al., 2008; Academy of Science of the Kyrgyz SSR, 1987) with means of -5.4 °C (station "Chatirkul") and -7.6 °C (station "TienShan") (Williams and Konovalov, 2008). The salinity of the lake water ranges from 1.06–1.15 g/l in the deeper western part of the lake to 0.24 g/l in the shallower eastern part near the inflow (Romanovsky, 2007). Measurements of oxygen concentrations (YSI Pro 6600 V2) during a field trip in July 2012 ranged from ~6 mg/l at the water surface to ~1 mg/l in 19 m depth with a clear oxygen minimum zone below ~11 m depth (Fig. 2). Water surface and bottom water temperatures (YSI Castaway CTD) at 19 m depth reached 13.2 °C and 9.4 °C. Specific conductivity (CTD) ranged from 1,902 µS/cm-1 at 19 m to 1,825 µS/cm-1, pH was ~9 (YSI Pro 6600 V2). Secchi depth was about 4 m. Nowadays, the lake is largely occupied by the amphipod *Gammarus alius* sp. nov. (Sidorov, 2012) and no fish live in the lake (Shnitnikov, 1978). The permafrost level is located at a depth of 2.5-3 m in the littoral coast zones and the lake is covered by ice from October to April (Shnitnikov, 1978). Several terraces in the north, south and east of the lake result from Pleistocene-Holocene lake level fluctuations (Romanovsky and Shatravin, 2007; Shnitnikov, 1978). Vegetation around the lake is generally poor and represented by high alpine meadows (Shnitnikov, 1978; Taft et al., 2011).

https://doi.org/10.5194/gchron-2019-18
Preprint. Discussion started: 20 January 2020

3. Methods

3.1 Coring and Composite profile

Five parallel cores each of 3 to 6 m length have been retrieved in 2012 from the deepest part of the lake (40°36.37' N, 75°14.02' E) by using an UWITEC piston corer (Fig. 1, Tab. 1). All cores were opened, split and photographed at GFZ Potsdam, where they are archived in a cool storage. A continuous composite profile of 623.5 cm length (CHAT12) was established by correlating the individual, overlapping cores via macroscopically visible marker layers (Fig. 3). Furthermore, seven parallel gravity cores (SC17_1-7) have been retrieved with a UWITEC gravity corer in 2017 (Fig.1, Tab.1) to recover the undisturbed sediment-water interface, from which the best preserved parallel core SC17_7 was used for gamma spectrometric analysis.

3.2 Sediment microfacies analysis and varve counting

10-cm-long sediment slabs with an overlap of 2 cm were continuously taken from the whole composite profile to prepare large-scale petrographic thin sections. Thin section preparation followed the method described by Brauer and Casanova (2001) and included freeze-drying and vacuum impregnation of the sediment slabs with Araldite epoxy resin. Microfacies analysis, including a semi-quantitative evaluation of planktic and periphytic diatoms, aquatic plant remains (e.g. *Potamogeton* sp., *Ruppia maritima*), ostracods, daphnia, characeae and chrysophytes, was carried out on a Zeiss Axioplan microscope using different magnifications (25–400 x) and included measurement of varve thicknesses, microfacies/varve type characterization, the definition of varve boundaries and the development of process-related deposition models. A varve quality index (VQI) ranging from 0-5 was given for each varve, comparable to the method from (Żarczyński et al., 2018) and references therein.

- VQI 0 = no varves or strongly disturbed varved sequences, no reliable counting (interpolation)
- VQI 1 = very low varve preservation, unclear and horizontally discontinuous varve and sublayer boundaries, difficult counting
- VQI 2 = low varve preservation, occasional horizontally discontinuous varve and sublayer boundaries, reliable counting
- VQI 3= medium varve preservation, horizontally continuous varve and sublayer boundaries, only small disturbances, reliable counting
- VQI 4= high varve preservation, clearly distinguishable varve and sublayer boundaries, reliable counting
- VQI 5= highest varve preservation, clearly distinguishable varve and sublayer boundaries, no disturbances, reliable counting

Varve counting was performed to establish a floating varve chronology. Non-varved intervals (VQI=0) between varved sediment sections were therefore interpolated by using the mean of sedimentation rates derived from about 20 varves above and below the non-varved part. Varves were counted twice by the same author. Counting uncertainty estimates were first assessed by the percentage deviation of the second to the first count within one thin section. The mean of these deviations was used as an overall counting uncertainty estimate and assigned to the entire varved record. The uncertainty estimates were thus also assigned to interpolated sequences.

https://doi.org/10.5194/gchron-2019-18
Preprint. Discussion started: 20 January 2020

3.3 Radiometric dating

3.3.1 Radiocarbon dating

In total, 36 accelerator mass spectrometry (AMS) ^{14}C measurements were carried out at the Poznań Radiocarbon Laboratory in Poland. Samples for ^{14}C measurements comprised two pieces of wood, bulk TOC samples, aquatic plant macro remains, daphnia remains and *Ruppia maritima* seeds (Tab.2). Additional samples of recent living daphnia and aquatic plants have been collected to assess the modern ^{14}C reservoir effect. The resulting conventional ^{14}C ages were calibrated using OxCal 4.3 (Ramsey, 2009) with the IntCal13 calibration curve (Reimer et al., 2013).

3.3.2 Gamma spectrometry dating

Gamma spectrometry measurements were performed on 0.5-cm-thick sediment slices that were continuously sampled from the upper 15.0 cm of gravity core SC17_7 (Suppl. Table. 1). The samples were freeze-dried and sieved through a 200 µm mesh for homogenization and removal of larger plant particles. Individual sample-aliquots were filled into gas-tight sealable low-activity Kryal© tubes at identical fill heights and accurately weighted. After sufficient ingrowth-time, the photo peak activities of ^{210}Pb ($T_{1/2}$= 22 a) and ^{214}Pb ($T_{1/2}$= 26.8 min), which is a daughter nuclide of ^{222}Rn ($T_{1/2}$= 3.8 d), were measured at 46.54, 295.24 and 351.93 keV. In addition, the photo peak activity of ^{137}Cs ($T_{1/2}$= 30.1 a) was measured at 661.66 keV. For this purpose, the Kryal© tubes were placed into two well-type germanium detectors G1 and G2 (Canberra Industries) (Schettler et al., 2006). Hardware control, data storage, and spectrum analysis were realized with the software Genie 2000 (Canberra Industries). The average counting uncertainty for ^{210}Pb was 5.9 %, for ^{214}Pb 7.7 % (295keV) and 3.7 % (351keV) and for ^{137}Cs 5.2 %. Efficiency calibrations were carried out for ^{210}Pb, ^{214}Pb and ^{137}Cs with the same analytical setup using a lab-internal standard and the "Loess Nussloch" standard (Potts et al., 2003). Blank activities for ^{137}Cs were negligible while average ^{210}Pb blank activities of 10 mBq/g for detector G2 and ^{214}Pb blank activities of 9 mBq/g for the detectors G1 and G2 were considered. The activity measurements of ^{214}Pb were used to quantify the proportion of supported ^{210}Pb ($^{210}Pb_{supp}$) produced by the decay of ^{226}Ra in the sediment. The activity of unsupported ^{210}Pb ($^{210}Pb_{unsupp}$) in the sediment, which originates from the decay of ^{222}Rn in the atmosphere and associated aeolian deposition, is quantified by the difference between measured $^{210}Pb_{total}$ and $^{210}Pb_{supp}$. We selected sections that showed linear correlations in the semi-logarithmic plot of $^{210}Pb_{unsupp}$ versus depth to infer average sedimentation rates using the constant initial concentration (CIC) model (c.f. Appleby, 2002)) (Suppl. Tab. 2). Intercalated sediment sections showed nearly uncorrelated ln($^{210}Pb_{unsupp}$) vs. depth relationships at 10.25–9.25, 6.25–4.25 and 2.25–1.75 cm depth (Suppl. Fig.2). Therefore, the initial $^{210}Pb_{unsupp}$ activities of samples that bridged these sections were used alternatively to determine time intervals between these samples to infer a chronology. To assess possible changes of the sedimentation regime we additionally calculated sedimentation rates of each 0.5-cm-thick sediment slice using the CRS model (constant initial $^{210}Pb_{unsupp}$ supply) (c.f. Appleby, 2002; Appleby and Oldfield, 1978) (Suppl. Tab.3).

https://doi.org/10.5194/gchron-2019-18
Preprint. Discussion started: 20 January 2020

4. Results

4.1 Lithology

The composite profile can be subdivided into six lithological units (Fig. 3). Lithozone (LZ) I from 623.5 to 566.0 cm depth consists of greyish-brownish clastic-calcareous sediments. It shows mm-scale laminations of fine sandy and silty to clayey layers. LZ II (566.0–480.0 cm) exhibits intercalations between horizons of very fine, mm-scale laminated brownish-reddish organic-rich sediments and sections with greyish calcareous sediments. Brownish-reddish intercalating horizons of mm-scale laminated organic and calcareous sediments characterize LZ III from 480.0 to 273.0 cm depth. LZ IV (273.0–130.0 cm) is characterized by brownish-reddish mm-scale laminated organic-rich sediments with intercalated horizons rich in aquatic plant remains, which occur at 232.0–223.0 cm, 185.0–180.0 cm and 164.0–130.0 cm depth. LZ V (130.0–41.0 cm depth) starts with a 16-cm-thick interval of dark grey mm-scale laminated calcareous sediments, followed by brown mm- to cm-scale laminated sediments until 41.0 cm depth. Laminations are only poorly preserved between 63.0 and 41.0 cm depth. The uppermost sediments of LZ VI (41.0–0.0 cm depth) consist of homogenous, brownish-greyish calcareous sediments, which are rich in aquatic plant remains. The uppermost centimetre is enriched in calcite and exhibits greyish faint laminations.

4.2 Sediment microfacies analysis

Microscopic sediment analysis revealed, that the macroscopically visible laminae below 63.0 cm depth, consist of mainly clastic laminations (Fig. 4). Clastic laminations intercalating with calcitic, aragonitic and organic sublayers build up cyclic successions. We used changing compositions of these sublayers to classify six clastic lamination subtypes described below. The subtypes were named according to the order of their dominant contents. Changing dominances of different sublayer successions reflect the lithozones.

4.2.1 Clastic-organic laminae

Clastic-organic laminae are present in all lithozones and most abundant in the record (42.5 % of all observed and measured laminae). This microfacies type is composed of four sublayers of which the most prominent is a basal clastic-detrital sublayer with a sharp lower boundary. The basal detrital sublayer contains mainly detrital calcite, which is distinguished from endogenic calcite by microscopic analyses. Detrital calcite is characterized by irregularly shaped gains and generally larger grain sizes of average of 0.6 mm and up to 1.82 mm in LZ I. Detrital layers further contain siliciclastic minerals as mica, quartz (qtz) and feldspars (fsp). This basal layer is often, but not regularly overlain by chrysophyte and/or diatom blooms and a third, mixed sublayer containing mainly fine-grained detrital calcite, mica, fsp and qtz with low amounts of endogenic calcite and varying amounts of diatom frustules, chrysophytes, characeae, ostracods and daphnia. The deposition cycle ends with a yellowish layer of amorphous organic material.

The mean thickness of clastic-organic laminae differs between the lithozones. In LZ I (Fig. 4 LZ I), the mean thickness is 0.59 mm with a maximum thickness of 3.1 mm. In LZ I, the basal detrital sublayer is thick and coarse-grained, rich in pyrite, and

https://doi.org/10.5194/gchron-2019-18
Preprint. Discussion started: 20 January 2020

contains mainly silt-to fine sand-sized grains and occasionally sand-sized qtz, calcite and fsp grains, whereas diatoms and chrysophytes are rare. In LZ II and III, clastic-organic laminae are less thick with a mean thickness of 0.27 mm and 0.48 mm respectively. In these lithozones, the basal sublayer contains no sand-sized particles. In LZ IV, mean varve thickness is 0.43 mm and the basal sublayer is often lens-shaped and horizontally discontinuous. In LZ V between 130.0 and 63.0 cm depth thickest clastic-organic laminae occur with a mean thickness of 1.5 mm and a maximum thickness of up to 7.0 mm (Fig. 4 LZ V). These clastic-organic laminae often include an additional detrital sublayer intercalated in the finer grained mixed sublayer.

4.2.2 Clastic-calcitic laminae

The second most common laminae subtype (23.5 %) are clastic-calcitic laminae (Fig. 4 LZ III lower part), which are most abundant in LZ I, II, III and V. This subtype is composed of four to five sublayers and the mean total thickness varies between 0.95 mm (LZ I), 0.35 mm (LZ II), 0.72 mm (LZ III), 1.56 mm (LZ IV) and the maximum value of 5.0 mm in LZ V. Clastic-calcitic laminae exhibit a basal detrital sublayer with a sharp lower boundary, which is followed by a bloom layer of chrysophytes and/or diatoms, occurring sporadically after and/or within the detrital sublayer. The third, overlying mixed sublayer contains medium amounts of endogenic as well as fine-grained detrital calcite, as well as mica, fsp and qtz grains but low amounts of diatom frustules and chrysophyte cysts. One depositional cycle typically ends with an amorphous organic matter sublayer. In LZ V, these clastic-calcitic laminae occasionally contain a very fine-grained, light greyish, micritic sublayer before the cycle ends with the amorphous organic sublayer.

4.2.3 Clastic-diatom laminae

Clastic-diatom laminae (20 %) occur in LZ II, III and IV. This subtype is composed of three sublayers and the mean thickness vary between 0.28 mm (LZ II), 0.34 mm (LZ III) and 0.35 mm (LZ IV). The depositional cycle starts with a basal detrital sublayer, which is overlain by a finer-grained mixed sublayer (detrital calcite, mica, fsp, qtz) occasionally containing chrysophytes and different diatom taxa. The third sublayer is formed by diatom blooms exclusively consisting of the planktic diatom species *Cyclotella choctawhatcheeana* (pers. comm. Anja Schwarz) (Fig. 4 LZ II upper part).

4.2.4 Clastic-aragonitic laminae

Clastic-aragonitic laminae are rare (2.7 %), mainly occur in LZ I and particularly at 600.0-605.0, and 609.0-616.0 cm composite depth. This subtype is composed of three sublayers and the mean thickness is 0.59 mm. These laminae exhibit the general pattern of clastic-organic laminae in LZ I, with a coarse-grained and thick basal detrital sublayer, but the overlying mixed (detrital calcite, mica, fsp, qtz and medium amounts of endogenic calcite) fine-grained sublayer additionally contains idiomorphic aragonite needles that are not found in clastic-organic varves. The sublayer succession ends with an amorphous organic matter sublayer.

https://doi.org/10.5194/gchron-2019-18
Preprint. Discussion started: 20 January 2020

4.2.5 Calcitic-clastic laminae

The deposition of calcitic-clastic laminae (6 %) with a dominating endogenic calcite sublayer is restricted to LZ II. This subtype is composed of three sublayers and the mean thickness is 0.41 mm, with a maximum of 2.0 mm. Calcitic–clastic laminae (Fig. 4 LZ II lower part) are usually characterized by a basal detrital sublayer which, however, is not developed in all calcitic-clastic laminae. The overlying sublayer generally exhibits low species abundancies of diatom frustules, chrysophyte cysts, aquatic plant remains, daphnia, ostracods and characeae but massive and fine-grained endogenic calcite, which is not the case in the clastic-calcitic laminae subtype. Endogenic calcite formed in the water column is recognized by its well-developed idiomorphic rhombohedral shapes. Scattered detrital grains occasionally occur within the endogenic calcite matrix. One depositional cycle ends with an amorphous organic matter sublayer.

4.2.6 Organic-clastic laminae

Horizons of organic-clastic laminae (5.2 %) with dominating organic sublayers are mainly present within LZ IV and V (Fig. 4 LZ IV) particular at 261.0-252.0, 176.0-173.0, 150.0-126.0 and 122.0-110.0 cm depth. This subtype is composed of three sublayers and the mean thickness is 0.49 mm (LZ IV) and 1.64 mm (LZ V) with a maximum of 9 mm in LZ V. Organic-clastic laminae exhibit an often horizontally discontinuous basal detrital sublayer (lens-shaped) in LZ IV, which is overlain by a mixed sublayer that contains detrital calcite, mica, fsp and qtz grains and many aquatic plant remains and periphytic diatoms (*Achnanthes brevipes*, pers. comm. Anja Schwarz), whose colony chains are often preserved. One deposition cyclic ends with a yellowish amorphous organic matter layer.

4.2.7 Homogenous sediments

The uppermost 41.0 cm of the sediment record consist of homogenous sediments, containing a fine-grained mix of autochthonous and allochthonous calcite, mica, qtz and fsp. The sediments are generally rich in organic remains, such as aquatic plant remains, chrysophytes, diatoms and chlorophytes (*Bracteacoccus*). Faint and discontinuous calcite laminae occur in the uppermost centimetre.

4.3 Chronology

4.3.1 Floating varve chronology (623.5-63.0 cm)

A floating varve chronology labelled as Chatvd19 (Fig. 5b) was established for the composite profile below 63.0 cm depth and comprises a total of 11,259 counted and interpolated varves. Based on the interpretation of laminations as varves, 9,026 of the total 11,259 varves were counted which is equal to 80.2 %. The first varve count reveals 9,026 varves and is the base for the floating varve chronology. Although the total varve number of 8,955 obtained by the second count is very similar to the first

https://doi.org/10.5194/gchron-2019-18
Preprint. Discussion started: 20 January 2020

count, larger deviations between the two varve counts in individual sediment sections occur throughout the sediment record due to varying stages of varve preservation as expressed in the VQI (Fig. 5a). Largest deviations occur in LZ I (603.0-595.0 cm) with 23.7 %, in LZ II (490.0-484.0 cm) with ~13 %, in LZ III (413.0-405.0 cm) with ~16 %, in LZ IV (141.0-134.0 cm depth) with 19.5 % and in LZ V (65.0-63.0 cm depth) with 7.7 %. Lowest deviations (<1 %) were obtained in LZ II at 539.0-530.0 cm and 498.0-490.0 cm, in LZ III at 451.0-445.0 cm, 421.0-413.0 cm, 375.0-369.0 cm, 299.0-290.0 cm and 282.0-275.0 cm, in LZ IV at 197.0-190.0 cm and in LZ V at 125.0-119.0 cm, 116.0-113.0 cm and 73.0-65.0 cm depth. Interpolated sequences are unevenly distributed within the record and are mainly present within LZ IV. The longest interpolated sequences occur in LZ IV with ~5 cm from 198.0-193.0 cm depth and in LZ III with almost 7 cm between 444.0-437.0 cm depth. A VQI (Fig.5a) of 1 is represented by 5.6 % of the total varves, VQI 2 by 8.4 %, VQI 3 by 26.4 %, VQI 4 by 18.3 % and VQI 5 by 21.4 %. The calculated mean deviation between the two varve counts of ~5 % (Fig. 5a) is used as a conservative uncertainty for the floating varve chronology to consider high uncertainties in individual sediment sections in a more realistic way, despite the similar total number of varves counted. The floating varve chronology has basal age of 11619 ± 603 years BP.

4.3.2 Chronology of the non-varved uppermost sediments

The uppermost 63.0 cm of the sediment profile are not varved and thus require alternative dating approaches including lead-210 dating, activity profiles of ^{137}Cs and sedimentation-rate based interpolation. First, we measured ^{210}Pb activity concentrations of the uppermost 15 cm of short core SC17_7 and applied the CIC and CRS models (Fig. 5c & 6, Suppl. Tab. 3). SC17_7 is correlated to the composite profile through a macroscopic facies change at 1.0 cm composite depth and through a laminated section from 45.0-41.0 cm composite depth (Suppl. Fig.1). The CIC and CRS-model based chronologies are broadly consistent and particularly date sediments at 8.75 cm (SC17_7) or 7.5 cm composite depth to AD 1945/46 (Fig. 5c and Fig. 6b, Suppl. Table 3,). This is in agreement with the onset of increased ^{137}Cs activity concentrations (Fig. 5c, 6c) marking the onset of nuclear weapon testing in AD 1945 (Ferm, 2000; Kudo et al., 1998; Norris and Arkin, 1998). Therefore, we applied the date of AD 1945 (8.75 cm in core SC17_7) as an anchor point for the chronology of the uppermost 63.0 cm of the composite profile. According to micro-facies based sedimentological correlation, this anchor point is located at 7.5 cm composite depth. The section of homogeneous sediments from this point down to 63.0 cm depth was interpolated. This interpolation is based on sedimentation rate calculations obtained by lead-210 dating and varve thickness measurements in adjacent sediment intervals. Calculations include sedimentation rates from the upper 7.5 cm (1.12 mm/yr), from 15 varves (1.9 mm/yr) between 41.0-63.0 cm depth and from 100 varves (1.66 mm/yr) below 63.0 cm depth and result in a mean SR of 1.56 mm/yr corresponding to 356 interpolated years. Adding the number of 356 interpolated years to the radiometric date of AD 1945 results in an age of AD 1589 (360 years BP) at 63.0 cm depth. We assume an uncertainty of ca. 10% for our interpolation. The anchor point thus has an age of 360 ± 40 years BP. The uncertainty of this anchor point is added to the varve counting uncertainty.

https://doi.org/10.5194/gchron-2019-18
Preprint. Discussion started: 20 January 2020

4.3.3 Radiocarbon dating

In total, we dated 36 samples of bulk organic carbon, daphnia remains, aquatic plant remains and *Ruppia martima* seeds. Only two samples were terrestrial plant remains (wood fragments) and sufficiently large to be used for AMS ^{14}C dating (Tab.2, Fig. 5 & 7). Except the two ages from terrestrial plant remains (Poz-54302 with 9988±203 and Poz-63307 with 6140 ± 137 cal yr BP), all other ages deviate from the varve chronology between 155 years at 0.0 cm depth and 6,150 years at 585.0 cm depth (Fig. 7). We observe a general trend of decreasing deviations up core with the maximum deviation of ~6,150 years at 585.0 cm depth in LZ I. Looking at more detail, the deviations between radiocarbon and varve ages exhibit a prominent step-wise increase particularly at the boundary between lithozone LZ IV and LZ V when it abruptly decreases from ~3,000 years to ~1,000 years. Modern aquatic plants collected during the field campaign in 2012 showed large modern reservoir ages of 330±30 and 2425±25 ^{14}C years and living daphnia yielded ages of 225±30 ^{14}C years.

5. Discussion

5.1 Interpretation of fine laminations as varves

The construction of varve chronologies relies on the proof of seasonal origin of fine laminations (Brauer et al., 2014; Ojala et al., 2012; Zolitschka et al., 2015). For the Chatyr Kol sediments a proof through modern observation in sediment traps is not possible because no varves are formed and preserved at present day. Therefore, we applied process-related deposition models (Fig. 4) based on detailed micro-facies analyses of the present types of fine laminations in petrographic thin sections and a comparison with varve types described in literature (Brauer, 2004; Zolitschka et al., 2015). Cyclic successions of mixed clastic laminations are observed throughout the Lake Chatyr Kol sediment record beneath 63.0 cm depth. We interpret the observed and previously described varying successions of different sublayers, forming subtypes of mixed clastic laminations, as resembling seasonally laminated sediments known from lakes which are located within carbonaceous catchments (Brauer and Casanova, 2001; Kelts and Hsü, 1978; Lauterbach et al., 2011; Lauterbach et al., 2019), at high altitudes and within glacial environments (Guyard et al., 2007; Leemann and Niessen, 1994). The observed succession of sublayers are interpreted as mixed varve types (clastic, -organic and –endogenic) (c.f. Zolitschka et al., 2015). Varve formation at Lake Chatyr Kol is related to the high seasonality of the local climate with an ice cover during winter and strong temperature gradients and varying precipitation amounts throughout the year affecting productivity, endogenic carbonate formation and local runoff. Varve preservation is promoted by the unique morphology of the deep western lake basin, where anoxic bottom water conditions can be maintained even under relatively low lake levels (Fig.2). We interpret the annual sedimentary cycle to always start with the deposition of a basal detrital sublayer with a sharp lower boundary which results from winter/spring snow and/or glacial melt (Guyard et al., 2007; Leemann and Niessen, 1994; Zolitschka et al., 2015) after the ice break-up in ~April (Shnitnikov, 1978). Runoff with suspended sediment load is then likely directed through the Kegagyr River in the east but may also be the result of laminar denudation. Basal detrital sublayers are generally overlain by blooms of chrysophytes and/or diatoms within clastic-

https://doi.org/10.5194/gchron-2019-18
Preprint. Discussion started: 20 January 2020

organic, organic-clastic, clastic-diatom and clastic-calcitic lamination/varve types. Chrysophytes and/or diatom blooms develop in consequence of available nutrients provided by spring overturn and spring/summer runoff in combination with rising temperatures during the summer season (Zolitschka et al., 2015). The productive phase in calcitic-clastic laminations/varves is however reflected by calcite precipitation. Calcite (endogenic, detrital and resuspended) is the main carbonate phase within the Chatyr Kol sediments. The formation of endogenic calcite in Lake Chatyr Kol can be related to 1) photosynthesis, where a high aquatic productivity lowers the concentrations of CO_2, increases the pH of the lake water and leads to a reduced solubility of CO_3^{2-}(Hodell et al., 1998; Kelts and Hsü, 1978; Zolitschka et al., 2015), 2) evaporation leading to an oversaturation of carbonate ions, and 3) weathering of the limestones and dolomites in the North which releases Ca^{2+} and HCO_3^- ions that are transported to the lake and thus increase their concentrations within the lake water (Wetzel, 2001). Aragonite precipitates were only overserved in the intervals between 600.0-605.0 and 609.0-616.0 cm composite depth. The formation of idiomorphic aragonite is either related to 1) strong evaporation or 2) to the amount of runoff and erosion of outcropping dolomites in the North, which affect the Mg/Ca ratio, where a Mg/Ca >12 favours the formation of aragonite and a Mg/Ca < 12 the formation of endogenic calcite (Kelts and Hsü, 1978; Müller et al., 1972). After the spring to early summer lake productivity, the deposition of a mixed sublayer consisting of finer, silt- to clay-sized detrital grains and low to medium amounts of endogenic calcite is observed in all lamination types, except within calcitic-clastic laminations. The mixed sublayer indicates resuspension of shore material to the core´s location due to e.g. wind induced wave activity and weak runoff during the ice-cover free season from ~April to October (Shnitnikov, 1978). The intercalation of discrete detrital layers within the mixed sublayer, as observed in clastic-organic laminae in LZ V, indicates pulses of runoff of suspended material which may be caused by rainfall events in summer (Aizen et al., 2001; Shnitnikov, 1978). One annual depositional cycle usually ends with the deposition of a thin sublayer of very fine amorphous organic matter which is deposited under quiet water conditions when the lake was ice covered. In lithozone V, an additional micritic sublayer is deposited before the amorphous organic sublayer at the end of the seasonal cycle in clastic-calcitic laminae when water turbulence is low.

5.2 Varve counting and chronology construction

The interpretation of different types of fine laminations allowed varve counting as a main tool for constructing the Chatyr Kol chronology largely based on incremental methods. Around 80% of the varves in the sediment record are double-counted in petrographic thin sections while the remaining part of ca 20% had to be interpolated based on sedimentation-rate estimates due to poor varve preservation. The resulting chronology comprises 11,259 years and is anchored to the absolute time scale at 63.0 cm sediment depth supported by a combination of lead-210 dating and occasional sedimentation rate measurements as described below. The resulting age-depth model is within uncertainties in good agreement with two calibrated AMS ^{14}C dates of wood pieces at 380.5 cm depth (6,140 ± 137 cal years BP; Poz-63307) and at 528.0 cm depth (9,988 ± 203 cal years BP; Poz-54302) (Fig. 5b, Tab. 2). The corresponding varve-based ages are 5,905 ± 320 years BP and 9,611 ± 505 years BP, respectively. As for all chronologies, uncertainties are inherent also to varve chronologies, which are commonly assessed via replicate counts (Brauer and Casanova, 2001; Lamoureux, 2001; Lotter and Lemcke, 1999; Ojala et al., 2012; Żarczyński et

https://doi.org/10.5194/gchron-2019-18
Preprint. Discussion started: 20 January 2020

al., 2018; Zolitschka et al., 2015). However, there is no standard procedure on how to calculate and present the uncertainties (Ojala et al., 2012; Zolitschka et al., 2015). Commonly, mean values of replicate count differences, the difference of maximum and minimum counts or their standard deviation are reported (Brauer et al., 2014; Ojala et al., 2012; Żarczyński et al., 2018; Zolitschka et al., 2015). Despite the inevitable increase of cumulative uncertainties with age or depth, systematic uncertainties arise and are caused by changes in varve preservation, strongly and abruptly varying sedimentation rates and the challenging differentiation of varve types with complex structures (Ojala et al., 2012; Żarczyński et al., 2018; Zolitschka et al., 2015). The overall very small difference between the two counts of the Chatyr Kol varved record of only -71 varves is due to the compensating effect between over-and underestimations of varve counts throughout the record. For the floating varve chronology we therefore compare the results for each individual thin section comprising 324 (506.8-497.6 cm) to 13 years (varves) (65.4-63.0 cm) (Fig. 5a, Fig. 8). Counting uncertainties for individual thin sections are reported as their percentage deviation from the first count used for the chronology and range between 0 and 23.7 % (Fig. 5a, Fig. 8). Largest deviations of 23.7 % in LZ I are caused by a low visibility of varve boundaries and by coring artefacts. Deviations of ~13 % in LZ II and of ~16 % in LZ III result from the abrupt intercalations between clastic-organic, clastic-diatom, clastic-calcitic and calcitic-clastic varve types with varying varve thicknesses (Fig. 4 LZ II & LZ III). Deviations in LZ IV with a maximum of 19.5 % coincide with generally lowest VQI values (Fig. 8) and result from the domination of clastic-organic and organic-clastic varves with lowest thicknesses and discontinuous basal detrital sublayers (Fig. 4 LZ IV) leading to generally higher counting uncertainties. Lowest deviations of <1 % in LZ II, LZ III, LZ IV and in LZ V represent best preservation and thus easily countable varves of different varve types. Generally, clastic-organic and clastic-calcitic varves with higher varve thickness, especially in LZ V are most reliably countable. The relatively high uncertainties of 7.7 % in LZ V are due to the low number of varves comprised in individual thin sections (Fig. 8). For the total uncertainty estimate for the floating varve chronology we use the mean of ± 5 % calculated from the uncertainties for each 10 cm interval. This conservative estimate is more realistic than the very low difference in the two repeated varve counts. An uncertainty of 5 % is in the range of elsewhere reported varve chronologies (Ojala et al., 2012).

Since the upmost 63.0 cm of the sediment profile are largely homogeneous, the varve chronology is floating and needs to be anchored to an absolute chronology at this point. The interpolation with a mean SR derived from the combination of the consistent CIC and CRS ^{210}Pb marker (AD 1945), the SR derived from discontinuously varved sequences between 41.0 and 63.0 cm depth and from 100 measured varves below 63.0 cm depth seems to be the best approach for constraining the uppermost age-depth relationship within the homogenous sediments, where further chronological markers are lacking. We are aware, that the interpolation-based "floating" anchor point at 63.0 cm depth is prone to additional uncertainties. We considered this by assuming a higher uncertainty of 10 % for this interval, than that of ± 5 % for the floating varve chronology.

5.3 Radiocarbon reservoir effects

Compared to the floating varve chronology, including two terrestrial (wood) AMS ^{14}C dates, we observed a general trend of decreasing reservoir effects of dated aquatic material up core with the maximum deviation of ~6,150 years at 585.0 cm depth

https://doi.org/10.5194/gchron-2019-18
Preprint. Discussion started: 20 January 2020

(10,930 ± 570 years BP) in LZ I (Fig. 7). The step-wise decrease of deviations between radiocarbon and varve ages is most pronounced at the boundary between lithozone LZ IV and LZ V, when it abruptly decreases from ~3,000 years to ~1,000 years. The reservoir effect generally depends on the rate of atmospheric CO_2 exchange between the water column and the air, internal mixing dynamics and the input of ^{14}C depleted carbonaceous material (Ascough et al., 2010; Jull et al., 2013; Keaveney and Reimer, 2012; Lockot et al., 2016; MacDonald et al., 1991). The catchment of Lake Chatyr Kol exhibits several sources that could be responsible for a ^{14}C-depletion of dissolved carbon species in the lake water. Highest reservoir ages in the early Holocene are likely the result of the combined influence of these sources: 1) the input of old, ^{14}C-depleted CO_2 with glacial meltwater (c.f. Hall and Henderson, 2001) at the onset of a warming Holocene and 2) the weathering and erosion of the northern outcropping limestones, which led to the release and input of dissolved bicarbonate to the lake (c.f. Abbott and Stafford, 1996; Hutchinson et al., 2004). Both processes lead to a ^{14}C-depleted CO_2 and HCO_3^-uptake during photosynthesis by e.g. submerged aquatic plants like *Ruppia martima* at 585.0 cm depth (Fig.7) and by phytoplankton, on which daphnia feed and which therefore also show similar reservoir effects. A high detrital input and thus a potentially high input of dissolved bicarbonate is supported by increased varve thicknesses during the early Holocene (Sect. 5.3.1, Fig. 9). Furthermore, 3) thawing of permafrost since the beginning of a warming Holocene might have released dissolved ^{14}C-depleted organic material and thus affect the ^{14}C TOC bulk measurements. Our fieldtrip observations and observations by Shnitnikov (1978) of modern permafrost reduction and the development of thermokarst in the southern part of the catchment around the neighbouring Lake Maloye support this assumption. The cause of a step-wise reservoir effect reduction is therefore likely also related to the combined effect of a generally decreasing glacial influence and a decreasing input of bicarbonate until ~AD 1150 at the boundary between LZ IV and LZ V (Fig.7, 9). The abrupt decrease of the reservoir affect after ~AD 1150, despite an increase in detrital carbonate supply (Sect. 5.3.5, Fig. 9) might be related to the silting up of the basin leading to a shallower water depth, which is more susceptible to water circulation and an enhanced atmospheric CO_2 exchange (c.f. Geyh et al., 1997).

5.4 Holocene variations in varve microfacies

The Lake Chatyr Kol sediment profile comprised six different varve types (Sect. 4.2, Fig. 4), which occurrences showed varying dominances in the different lithozones which are described below. The individual lithozones always comprised more than one varve type (Fig. 9) with a maximum of five different varve types occurring in LZ III and II to three varve types in LZ V.

5.4.1 Lithozone I (623.5-566.0 cm: 11,619 ± 603 to 10,730 ± 560 years BP)

Lithozone I is characterized by relatively high and varying varve thicknesses and by the presence of clastic-organic, clastic-calcitic and clastic-aragonite varves (Fig. 9 LZ I). Clastic-organic varves constitute about 57 % of the observed and counted varve types, clastic-calcitic 29 % and clastic-aragonitic 14 %. Generally thick detrital coarse-grained spring sublayers, which were observed in all varve types in this LZ, are indicative for intense runoff by winter/spring snow meltwater and/or by glacial

https://doi.org/10.5194/gchron-2019-18
Preprint. Discussion started: 20 January 2020

thawing during summer (Shnitnikov, 1978) caused by highest insolation (Berger and Loutre, 1991; Chen et al., 2008; Jin et al., 2011; Li and Morrill, 2010) at the onset of a warming early Holocene. Glaciers of the inner Tian Shan started to retreat between ~12-8 ka years BP (Bondarev, 1997; Shnitnikov, 1978) causing enhanced detrital input into the lake. The low species abundancies of aquatic plants (*Ruppia Maritima or Potamogeton* sp.), daphnia and characeae reflect a littoral community and indicate a low aquatic productivity and a relative low lake level during this time. Clastic-calcitic varves appear at the base of the composite profile and towards the end of LZ I, whereas clastic-aragonitic varves dominate in the period from ~11,500 to 11,000 years BP. The formation of idiomorphic aragonite within the summer sublayer indicates evaporative conditions. Aragonite formation further requires input of Mg-rich carbonates to constitute a Mg/Ca ratio >12 favourable for aragonite formation (Kelts and Hsü, 1978; Müller et al., 1972).

5.4.2 Lithozone II (566.0-480.0 cm: 10,730 ± 560 to 8,040 ± 430 years BP)

In this lithozone calcitic-clastic varves constitute about 21 % of the observed varves and clastic-calcitic varves ~22 %, while clastic-organic varves make up ~42 % and clastic-diatom varves ~15%. This lithozone is characterized by intercalations of calcitic varve types (calcitic-clastic & clastic-calcitic) with clastic-organic and clastic-diatom varves (Fig. 4 LZ II) which show decadal- to centennial periodicities. The periodic occurrence of intensified calcite formation could reflect intervals of increased productivity or summer temperatures that might have been triggered by solar activity variations as observed in tree ring data from the Tian Shan (Raspopov et al., 2008). The shift in endogenic carbonate type from aragonite to dominating calcite at ~10,730 years BP (Fig. 9 LZ II) coincides with an increase in biological activity, as inferred from increased abundancies of e.g. chrysophytes, diatoms and characeae (Fig. 9) and thus suggests biologically induced calcite precipitation resulting from photosynthesis (Zolitschka et al., 2015). The establishment of a diverse lake fauna, as seen in the high abundancies of chrysophytes, planktic (*Cyclotella choctawhatcheeana)* and periphytic diatoms (*Achnanthes brevipes*) and aquatic plants, ostracods, characeae and few daphnia indicate favourable summer conditions. The mixed littoral and pelagic species assemblage is interpreted as an indication of a low lake level.

5.4.3 Lithozone III (480.0-273.0 cm: 8,040 ± 350 to 4,140 ± 230 years BP)

The deposition of clastic-calcitic varves corresponds to ~38 % of the observed varves in this lithozone, while clastic-organic varves make up ~27 % and clastic-diatom varves ~34 %. Clastic-calcite varves are generally thicker than the other varve types of this LZ mainly because of exceptionally thick summer sublayers. These summer layers consist of endogenic calcite mixed with fine-grained detrital grains. Therefore, these varves likely reflect increased resuspension due to wind induced wave activity. As in LZ II, a decadal- to centennial-scale alternation of clastic-diatom, clastic-organic and clastic-calcitic varves is characteristic also for this lithozone (Fig.4 LZ III, Fig. 9 LZ III). At ~8,040 years BP the deposition of calcitic-clastic varves ceased and are replaced by clastic-calcitic, clastic-organic and clastic-diatom varves probably because of lower summer temperatures due to decreasing summer insolation (Berger and Loutre, 1991; Chen et al., 2008; Jin et al., 2011; Li and Morrill, 2010) and relatively reduced Ca^{2+}, HCO_3^-, and CO_3^2 concentrations due to a high lake level. Higher lake levels are supported

https://doi.org/10.5194/gchron-2019-18
Preprint. Discussion started: 20 January 2020

by the dominance of planktic diatoms and the occurrence of lake deposits at the eastern and southern shore which have been dated from 6,688 ± 473 to 4,621 ± 594 cal years BP (^{14}C ages published by Shnitnikov (1978) calibrated with OxCal4.3 & IntCal13). During our field work we found lake sediments on a shallow terrace ~7 m above the current lake level east of the lake which also revealed a mid-Holocene age of 5,786 ± 122 cal years BP (Poz-109830 Tab.2). Higher lake levels at that time have been explained by glacier retreat in the catchment (Bondarev, 1997; Shnitnikov, 1978). However, more recently even minor glacial advances in the Aksai Basin east of the Chatyr Kol catchment ^{10}Be exposure dated between 7.5 and ~4.5 ka were reported (Koppes et al., 2008).

5.4.4 Lithozone IV (273.0-130.0 cm: 4,140 ± 230 to 800 ± 60 years BP/ AD 1150 ± 60

This Lithozone contains clastic-organic (58 %), organic-clastic (18 %), clastic-diatom (17 %) and clastic-calcitic varves (6 %) (Fig. 9 LZ IV). High abundancies of planktic diatoms as well as clastic-diatom varves prevail until ~2,900 years BP, whereas clastic-organic and organic-clastic varves with abundant aquatic plant remains and periphytic diatoms occur afterwards and dominate the sediments particularly after ~2,200 years BP. Abundant aquatic plant remains and periphytic diatoms can be explained by reworking due to wave activity and water column mixing during low lake levels. Low lake levels are inferred from the modern observation that aquatic plants occupy the shallow parts of the Lake from ~15.0 to 0.5 m. A decreased lake level combined with the shallow bathymetry of the lake basin (Fig, 1) further promotes large impacts on the species communities, which supports the changing abundancies from a planktic to a littoral dominated fauna and flora after ~2,200 years BP. An increased mixing of the water body also caused a clear decline in varve preservation. The rate of detrital input as observed in clastic-organic, organic-clastic varves (Fig. 4 LZ IV) is rather constant and mainly appears within the spring sublayer suggesting stable snow melt runoff from 4140 years BP to AD 1150. At ~2,600 and at 2,300 years BP clastic-calcite varves with thickened summer sublayers appear for a few decades indicating enhanced summer runoff.

5.4.5 Lithozone V (130.0-41.0 cm: AD 1150 ± 60 to AD 1730 ± 30)

Clastic-organic varves constitute 59 % of the observed varves in LZ V, clastic-calcitic varves 26 % and organic-clastic varves 15 %, the latter ceasing at 110.5 cm (AD 1260 ± 50). Varve microfacies changes abruptly at 130 cm depth or AD 1150 from the dominance of organic-clastic varves to dominating clastic-organic and clastic-calcitic varves. Within 5 years, varve thickness drastically increase from Ø 0.43 mm in LZ IV to Ø 1.52 mm in LZ V due to thicker summer sublayers, which frequently contain additional runoff layers (Fig. 4 LZ V) indicating an increase in summer precipitation events. Increased precipitation should have caused a lake level rise, which is supported by the presence of paleo lake deposits at the northern and eastern shores dated at 530 ± 204 cal years BP, 906 ± 160 and 1,097 ± 166 cal years BP (Shnitnikov, 1978) and by well-preserved varves due to prevailing anoxic bottom water conditions (Zolitschka et al., 2015).

https://doi.org/10.5194/gchron-2019-18
Preprint. Discussion started: 20 January 2020

5.4.6 Lithozone VI (41.0-0.0 cm: AD 1730 ± 30 to AD 2012)

At around AD 1730 ± 30 varve formation and/or preservation ceased and sediments became predominantly homogeneous. The cessation of varves might be related to enhanced mixing of the water column resulting in a loss of the oxygen minimum zone (Fig.2a) caused by decreasing water depth due to silting–up, which accelerated with the abrupt increase in sedimentation rate at AD 1150 and/or due to strengthening of the wind conditions and wave activity.

6. Conclusion

We present the first varved lake sediment record in arid Central Asia that covers almost the entire Holocene. The established floating varve chronology provides an independent dating for a setting with scarce material for radiocarbon dating. This chronology is considered a robust fundament for further detailed palaeoenvironmental and palaeoclimatic reconstructions. Furthermore, the independent layer counting chronology allows detection of pronounced changes in radiocarbon reservoir ages throughout the Holocene. The largest reservoir effect of ~6150 years in the early Holocene is likely caused by glacial melt and enhanced local erosion resulting in a surplus of dead carbon. Lower reservoir ages of ~1000 years and less in the late Holocene might be related to enhanced atmospheric CO_2 exchange when the lake was shallower due to silting-up of the lake basin and/or increased windiness. The construction of the varve-based chronology was only possible through detailed micro-facies analyses of the entire sediment sequence in overlapping thin sections which allowed developing seasonal deposition models for all observed types of fine laminations. Based on these models and their comparison with published varve micro-facies data, we interpret all six Chatyr Kol lamination types as varves. Compared to many other varved lake sediment records, the Chatyr Kol varves are very heterogeneous and a complex pattern of six different micro-facies types developed throughout the Holocene. All varve types are predominantly clastic and comprise variations of their summer sublayers with changing dominances of organic, diatom, calcitic, aragonitic and additional detrital sublayers. Varve thickness changed accordingly with the varve micro-facies types, whereby the most conspicuous increase of varve thickness occurred at AD 1150 which is caused by increased erosion and runoff likely triggered by higher summer precipitation. The increase in detrital input into the lake further caused an acceleration of the silting-up processes. The complex succession and variations of varve types throughout the Holocene with some major change points still requires further detailed investigations and interpretation together with other proxy data.

Data availability

The presented data will be provided through PANGAEA.

https://doi.org/10.5194/gchron-2019-18
Preprint. Discussion started: 20 January 2020

Competing interest

The authors declare that they have no conflict of interest.

Authors contributions

JK performed the microfacies analysis, ^{210}Pb and ^{137}Cs gamma spectrometry and wrote the manuscript with contributions from all co-authors. JM designed the project and organised field work. SL carried out sediment coring and was responsible for ^{14}C dating. RU provided information about the catchment geology and lake level changes. AB supervised analyses and manuscript writing.

Acknowledgements

We thank S. Lauterbach, S. Pinkerneil, M. Köhler, R. Schedel, and D. Henning for retrieving the long piston cores from Lake Chatyr Kol in 2012 in the framework of the project CADY (Central Asian Climate Dynamics). S. Pinkerneil and Y. Beutlich are thanked for help with the geochemical analyses. S. Orunbaev, M. Daiyrov, S. Kalmuratov, G. Omurova and K, Jusupova are acknowledged for their support during field trips. We further thank T Goslar for AMS ^{14}C dating and D. Berger, G. Arnold and B. Brademann for thin section preparation and G. Schettler for his help with lead-210 dating.

Funding

This study was conducted in the framework of CAHOL (Central Asian HOLocene), a subproject of the joint project CAME II (Central Asia Climate Tipping Points and their Consequences) funded by the German Federal Ministry of Education (BMBF) through grant 03G0864B. The study further contributes to the Helmholtz Climate Initiative REKLIM Topic 8 'Abrupt climate change derived from proxy data'.

References

Abbott, M. B. and Stafford, T. W.: Radiocarbon geochemistry of modern and ancient Arctic lake systems, Baffin Island, Canada, Quaternary Research, 45, 300-311, https://doi.org/10.1006/qres.1996.0031, 1996.

Academy of Science of the Kyrgyz SSR: Atlas of the Kyrgyz Soviet Socialistic Republic: Natural conditions and resources, State Agency of Cartography and Geodesy, Central Directorate for Geodesy and Cartography, Council of Minister of the USSR, Moscow, 1987

Aizen, E. M., B., A. V., M., M. J., Nakamura, T., and Ohta, T.: Precipitation and atmospheric circulation patterns at mid-latitudes of Asia, International Journal of Climatology, 21, 21, https://doi.org/10.1002/joc.626, 2001.

Aizen, V. B.: Association between atmospheric circulation patterns and firn-ice core records from the Inilchek glacierized area, central Tien Shan, Asia, Journal of Geophysical Research, 109, https://doi.org/10.1029/2003JD003894, 2004.

Appleby, P.: Chronostratigraphic techniques in recent sediments. In: Tracking environmental change using lake sediments, Springer, https://doi.org/10.1007/0-306-47669-X_9, 2002.

Appleby, P. and Oldfield, F.: The calculation of lead-210 dates assuming a constant rate of supply of unsupported 210Pb to the sediment, Catena, 5, 1-8, https://doi.org/10.1016/S0341-8162(78)80002-2, 1978.

https://doi.org/10.5194/gchron-2019-18
Preprint. Discussion started: 20 January 2020

Ascough, P., Cook, G., Church, M., Dunbar, E., Einarsson, Á., McGovern, T., Dugmore, A., Perdikaris, S., Hastie, H., and Friðriksson, A.: Temporal and spatial variations in freshwater 14 C reservoir effects: Lake Mývatn, northern Iceland, Radiocarbon, 52, 1098-1112, https://doi.org/10.1017/S003382220004618X, 2010.

Berger, A. and Loutre, M.-F.: Insolation values for the climate of the last 10 million years, Quaternary Science Reviews, 10, 297-317, https://doi.org/10.1016/0277-3791(91)90033-Q, 1991.

Bondarev, L. G.: Fluctuations of local glaciers in the southern ranges of the former USSR: 18,000-8000 BP, https://doi.org/10.1016/S1040-6182(96)00023-7, 1997.

Boomer, I., Aladin, N., Plotnikov, I., and Whatley, R.: The palaeolimnology of the Aral Sea: a review, Quaternary Science Reviews, 19, 1259-1278, https://doi.org/10.1016/S0277-3791(00)00002-0, 2000.

Brauer, A.: Annually Laminated Lake Sediments and Their Palaeoclimatic Relevance. In: The Climate in Historical Times: Towards a Synthesis of Holocene Proxy Data and Climate Models, Fischer, H., Kumke, T., Lohmann, G., Flöser, G., Miller, H., von Storch, H., and Negendank, J. F. W. (Eds.), Springer Berlin Heidelberg, Berlin, Heidelberg, https://doi.org/10.1007/978-3-662-10313-5_7, 2004.

Brauer, A. and Casanova, J.: Chronology and depositional processes of the laminated sediment record from Lac d'Annecy, French Alps, Journal of Paleolimnology, 25, 163-177, https://doi.org/10.1023/A:1008136029735, 2001.

Brauer, A., Hajdas, I., Blockley, S. P. E., Bronk Ramsey, C., Christl, M., Ivy-Ochs, S., Moseley, G. E., Nowaczyk, N. N., Rasmussen, S. O., Roberts, H. M., Spötl, C., Staff, R. A., and Svensson, A.: The importance of independent chronology in integrating records of past climate change for the 60–8 ka INTIMATE time interval, Quaternary Science Reviews, 106, 47-66, https://doi.org/10.1016/j.quascirev.2014.07.006, 2014.

Chen, F., Yu, Z., Yang, M., Ito, E., Wang, S., Madsen, D. B., Huang, X., Zhao, Y., Sato, T., John B. Birks, H., Boomer, I., Chen, J., An, C., and Wünnemann, B.: Holocene moisture evolution in arid central Asia and its out-of-phase relationship with Asian monsoon history, Quaternary Science Reviews, 27, 351-364, https://doi.org/10.1016/j.quascirev.2007.10.017, 2008.

De Grave, J., Glorie, S., Buslov, M. M., Izmer, A., Fournier-Carrie, A., Batalev, V. Y., Vanhaecke, F., Elburg, M., and Van den haute, P.: The thermo-tectonic history of the Song-Kul plateau, Kyrgyz Tien Shan: Constraints by apatite and titanite thermochronometry and zircon U/Pb dating, Gondwana Research, 20, 745-763, https://doi.org/10.1016/j.gr.2011.03.011, 2011.

Esper, J., Shiyatov, S. G., Mazepa, V. S., Wilson, R. J. S., Graybill, D. A., and Funkhouser, G.: Temperature-sensitive Tien Shan tree ring chronologies show multi-centennial growth trends, Climate Dynamics, 21, 699-706, https://doi.org/10.1007/s00382-003-0356-y, 2003.

Ferm, B.: Nuclear Explosions 1945-1998, 2000.

Fohlmeister, J., Plessen, B., Dudashvili, A. S., Tjallingii, R., Wolff, C., Gafurov, A., and Cheng, H.: Winter precipitation changes during the Medieval Climate Anomaly and the Little Ice Age in arid Central Asia, Quaternary Science Reviews, 178, 24-36, https://doi.org/10.1016/j.quascirev.2017.10.026, 2017.

Geyh, M. A., Schotterer, U., and Grosjean, M.: Temporal changes of the 14 C reservoir effect in lakes, Radiocarbon, 40, 921-931, https://doi.org/10.1017/S0033822200018890, 1997.

Guyard, H., Chapron, E., St-Onge, G., Anselmetti, F. S., Arnaud, F., Magand, O., Francus, P., and Mélières, M.-A.: High-altitude varve records of abrupt environmental changes and mining activity over the last 4000 years in the Western French Alps (Lake Bramant, Grandes Rousses Massif), Quaternary Science Reviews, 26, 2644-2660, https://doi.org/10.1016/j.quascirev.2007.07.007, 2007.

Hall, B. L. and Henderson, G. M.: Use of uranium–thorium dating to determine past 14C reservoir effects in lakes: examples from Antarctica, Earth and Planetary Science Letters, 193, 565-577, https://doi.org/10.1016/S0012-821X(01)00524-6, 2001.

Heinecke, L., Mischke, S., Adler, K., Barth, A., Biskaborn, B. K., Plessen, B., Nitze, I., Kuhn, G., Rajabov, I., and Herzschuh, U.: Climatic and limnological changes at Lake Karakul (Tajikistan) during the last ~29 cal ka, Journal of Paleolimnology, 58, 317-334, https://doi.org/10.1007/s10933-017-9980-0, 2017.

Herzschuh, U.: Palaeo-moisture evolution in monsoonal Central Asia during the last 50,000 years, Quaternary Science Reviews, 25, 163-178, https://doi.org/10.1016/j.quascirev.2005.02.006, 2006.

Hodell, D. A., Schelske, C. L., Fahnenstiel, G. L., and Robbins, L. L.: Biologically induced calcite and its isotopic composition in Lake Ontario, Limnology and Oceanography, 43, 187-199, https://doi.org/10.4319/lo.1998.43.2.0187, 1998.

Hou, J., D'Andrea, W. J., and Liu, Z.: The influence of 14C reservoir age on interpretation of paleolimnological records from the Tibetan Plateau, Quaternary Science Reviews, 48, 67-79, https://doi.org/10.1016/j.quascirev.2012.06.008, 2012.

Huayu, L., Cunfa, Z., Mason, J., Shuangwen, Y., Hua, Z., Yali, Z., Junfeng, J., Swinehart, J., and Chengmin, W.: Holocene climatic changes revealed by aeolian deposits from the Qinghai Lake area (northeastern Qinghai-Tibetan Plateau) and possible forcing mechanisms, The Holocene, 21, 297-304, https://doi.org/10.1177/0959683610378884, 2010.

Hutchinson, I., James, T. S., Reimer, P. J., Bornhold, B. D., and Clague, J. J.: Marine and limnic radiocarbon reservoir corrections for studies of late-and postglacial environments in Georgia Basin and Puget Lowland, British Columbia, Canada and Washington, USA☆, Quaternary Research, 61, 193-203, https://doi.org/10.1016/j.yqres.2003.10.004, 2004.

Jarvis, A.: Hole-field seamless SRTM data, International Centre for Tropical Agriculture (CIAT), http://srtm. csi. cgiar. org, 2008.

https://doi.org/10.5194/gchron-2019-18
Preprint. Discussion started: 20 January 2020

Jin, L., Chen, F., Morrill, C., Otto-Bliesner, B. L., and Rosenbloom, N.: Causes of early Holocene desertification in arid central Asia, Climate Dynamics, 38, 1577-1591, https://doi.org/10.1007/s00382-011-1086-1, 2011.

Jull, A. J. T., Burr, G. S., and Hodgins, G. W. L.: Radiocarbon dating, reservoir effects, and calibration, Quaternary International, 299, 64-71, https://doi.org/10.1016/j.quaint.2012.10.028, 2013.

Keaveney, E. M. and Reimer, P. J.: Understanding the variability in freshwater radiocarbon reservoir offsets: a cautionary tale, Journal of Archaeological Science, 39, 1306-1316, https://doi.org/10.1016/j.jas.2011.12.025, 2012.

Kelts, K. and Hsü, K.: Freshwater carbonate sedimentation. In: Lakes, Springer, https://doi.org/10.1007/978-1-4757-1152-3_9, 1978.

Koppes, M., Gillespie, A. R., Burke, R. M., Thompson, S. C., and Stone, J.: Late Quaternary glaciation in the Kyrgyz Tien Shan, Quaternary Science Reviews, 27, 846-866, https://doi.org/10.1016/j.quascirev.2008.01.009, 2008.

Kudo, A., Zheng, J., Koerner, R., Fisher, D., Santry, D., Mahara, Y., and Sugahara, M.: Global transport rates of 137Cs and 239+ 240Pu originating from the Nagasaki A-bomb in 1945 as determined from analysis of Canadian Arctic ice cores, Journal of environmental radioactivity, 40, 289-298, https://doi.org/10.1016/S0265-931X(97)00023-4, 1998.

Lamoureux, S.: Varve Chronology Techniques. In: Tracking Environmental Change Using Lake Sediments: Basin Analysis, Coring, and Chronological Techniques, Last, W. M. and Smol, J. P. (Eds.), Springer Netherlands, Dordrecht, https://doi.org/10.1007/0-306-47669-X_11, 2001.

Lauterbach, S., Brauer, A., Andersen, N., Danielopol, D. L., Dulski, P., Hüls, M., Milecka, K., Namiotko, T., Obremska, M., and Von Grafenstein, U.: Environmental responses to Lateglacial climatic fluctuations recorded in the sediments of pre-Alpine Lake Mondsee (northeastern Alps), Journal of Quaternary Science, 26, 253-267, https://doi.org/10.1002/jqs.1448, 2011.

Lauterbach, S., Mingram, J., Schettler, G., and Orunbaev, S.: Two twentieth-century MLH = 7.5 earthquakes recorded in annually laminated lake sediments from Sary Chelek, western Tian Shan, Kyrgyzstan, Quaternary Research, 92, 288-303, https://doi.org/10.1017/qua.2019.21, 2019.

Lauterbach, S., Witt, R., Plessen, B., Dulski, P., Prasad, S., Mingram, J., Gleixner, G., Hettler-Riedel, S., Stebich, M., and Schnetger, B.: Climatic imprint of the mid-latitude Westerlies in the Central Tian Shan of Kyrgyzstan and teleconnections to North Atlantic climate variability during the last 6000 years, The Holocene, 24, 970-984, https://doi.org/10.1177/0959683614534741, 2014.

Leemann, A. and Niessen, F.: Holocene glacial activity and climatic variations in the Swiss Alps: reconstructing a continuous record from proglacial lake sediments, The Holocene, 4, 259-268, https://doi.org/10.1177/095968369400400305, 1994.

Li, Y. and Morrill, C.: Multiple factors causing Holocene lake-level change in monsoonal and arid central Asia as identified by model experiments, Climate Dynamics, 35, 1119-1132, https://doi.org/10.1007/s00382-010-0861-8, 2010.

Lockot, G., Ramisch, A., Wünnemann, B., Hartmann, K., Haberzettl, T., Chen, H., and Diekmann, B.: A Process- and Provenance-Based Attempt to Unravel Inconsistent Radiocarbon Chronologies in Lake Sediments: An Example from Lake Heihai, North Tibetan Plateau (China), Radiocarbon, 57, 1003-1019, https://doi.org/10.2458/azu_rc.57.18221, 2016.

Lotter, A. F. and Lemcke, G.: Methods for preparing and counting biochemical varves, Boreas, 28, 243-252, https://doi.org/10.1111/j.1502-3885.1999.tb00218.x, 1999.

MacDonald, G. M., Beukens, R. P., and Kieser, W.: Radiocarbon dating of limnic sediments: a comparative analysis and discussion, Ecology, 72, 1150-1155, https://doi.org/10.2307/1940612, 1991.

Mathis, M., Sorrel, P., Klotz, S., Huang, X., and Oberhänsli, H.: Regional vegetation patterns at lake Son Kul reveal Holocene climatic variability in central Tien Shan (Kyrgyzstan, Central Asia), Quaternary Science Reviews, 89, 169-185, https://doi.org/10.1016/j.quascirev.2014.01.023, 2014.

Mischke, S., Liu, C., Zhang, J., Zhang, C., Zhang, H., Jiao, P., and Plessen, B.: The world's earliest Aral-Sea type disaster: the decline of the Loulan Kingdom in the Tarim Basin, Scientific Reports, 7, 43102, https://doi.org/10.1038/srep43102, 2017.

Mischke, S., Weynell, M., Zhang, C., and Wiechert, U.: Spatial variability of 14C reservoir effects in Tibetan Plateau lakes, Quaternary International, 313-314, 147-155, https://doi.org/10.1016/j.quaint.2013.01.030, 2013.

Müller, G., Irion, G., and Förstner, U.: Formation and diagenesis of inorganic Ca− Mg carbonates in the lacustrine environment, Naturwissenschaften, 59, 158-164, 1972.

Norris, R. S. and Arkin, W. M.: Known nuclear tests worldwide, 1945-98, Bulletin of the Atomic Scientists, 54, 65-68, 1998.

Ojala, A. E. K., Francus, P., Zolitschka, B., Besonen, M., and Lamoureux, S. F.: Characteristics of sedimentary varve chronologies – A review, Quaternary Science Reviews, 43, 45-60, https://doi.org/10.1016/j.quascirev.2012.04.006, 2012.

Peck: Mid to Late Holocene climate change in north central Mongolia as recorded in the sediments of Lake Telmen, https://doi.org/10.1016/S0031-0182(01)00465-5, 2002.

Potts, P. J., Thompson, M., Chenery, S. R., Webb, P. C., and Kasper, H. U.: GeoPT13-An international proficiency test for analytical geochemistry laboratories-report on round 13/July 2003 (Köln Loess), International Association of Geoanalysts, 2003.

Ramsey, C. B.: Bayesian analysis of radiocarbon dates, Radiocarbon, 51, 337-360, https://doi.org/10.1017/S0033822200033865, 2009.

Rasmussen, K., Ricketts, R., Johnson, T., Romanovsky, V., and Grigina, O.: An 11,000-year history of Central Asian paleoclimate change recorded in deep sediments of Lake Issyk-Kul, Kyrgyzstan, Eos Trans. AGU, 81, 2000.

https://doi.org/10.5194/gchron-2019-18
Preprint. Discussion started: 20 January 2020

Raspopov, O. M., Dergachev, V. A., Esper, J., Kozyreva, O. V., Frank, D., Ogurtsov, M., Kolström, T., and Shao, X.: The influence of the de Vries (~200-year) solar cycle on climate variations: Results from the Central Asian Mountains and their global link, Palaeogeography, Palaeoclimatology, Palaeoecology, 259, 6-16, https://doi.org/10.1016/j.palaeo.2006.12.017, 2008.

Reference Book of Climate USSR, Kyrygz SSR, Hydrometeo Publishings, Leningrad, 1988.

Reimer, P. J., Bard, E., Bayliss, A., Beck, J. W., Blackwell, P. G., Ramsey, C. B., Buck, C. E., Cheng, H., Edwards, R. L., and Friedrich, M.: IntCal13 and Marine13 radiocarbon age calibration curves 0–50,000 years cal BP, Radiocarbon, 55, 1869-1887, https://doi.org/10.2458/azu_js_rc.55.16947, 2013.

Ricketts, R. D., Johnson, T. C., Brown, E. T., Rasmussen, K. A., and Romanovsky, V. V.: The Holocene paleolimnology of Lake Issyk-Kul, Kyrgyzstan: trace element and stable isotope composition of ostracodes, Palaeogeography, Palaeoclimatology, Palaeoecology, 176, 207-227, https://doi.org/10.1016/S0031-0182(01)00339-X, 2001.

Romanovsky, V. V.: Climate, Glaciers, Lakes of Tien Shan: Journey of the past, 2007.

Romanovsky, V. V. and Shatravin, V. I.: Reconstruction of glacial and climate changes in the late Pleistocene and Holocene based on studies of closed alpine lakes in the Tien Shan and Pamir, 2007.

Schettler, G., Mingram, J., Negendank, J. F. W., and Jiaqi, L.: Palaeovariations in the East-Asian Monsoon Regime Geochemically Recorded in Varved Sediments of Lake Sihailongwan (Northeast China, Jilin Province). Part 2: a 200-Year Record of Atmospheric Lead-210 Flux Variations and its Palaeoclimatic Implications, Journal of Paleolimnology, 35, 271-288, https://doi.org/10.1007/s10933-005-0102-z, 2006.

Schröter, N., Lauterbach, S., Kalanke, J., Mingram, J., Yildizd, C., Schoutend, S., and Gleixner, G.: Biomolecular evidence of early human occupation of a high-altitude site in Western Central Asia during the Holocene. In:Frontiers in Earth Science, 2019.

Schwarz, A., Turner, F., Lauterbach, S., Plessen, B., Krahn, K. J., Glodniok, S., Mischke, S., Stebich, M., Witt, R., and Mingram, J.: Mid- to late Holocene climate-driven regime shifts inferred from diatom, ostracod and stable isotope records from Lake Son Kol (Central Tian Shan, Kyrgyzstan), Quaternary Science Reviews, 177, 340-356, https://doi.org/10.1016/j.quascirev.2017.10.009, 2017.

Shnitnikov, A. V.: Paleolimnology of Chatyrkel Lake (Tien-Shan), Polskie Archwium HydrobiologII, 25, 1978.

Sidorov, D. A.: Two new species of freshwater amphipods (Crustacea: Gammaridae) from Central Asia, with comments on the unusual upper lip morphology, Zootaxa, 3317, 1-24, http://dx.doi.org/10.11646/zootaxa.3317.1.1, 2012.

Taft, J. B., Phillippe, L. R., Dietrich, C. H., and Robertson, K. R.: Grassland composition, structure, and diversity patterns along major environmental gradients in the Central Tien Shan, Plant Ecology, 212, 1349-1361, https://doi.org/10.1007/s11258-011-9911-5, 2011.

Wetzel, R. G.: Limnology: lake and river ecosystems, Gulf Professional Publishing, 2001.

Williams, M. and Konovalov, V.: Central Asia temperature and precipitation data, 1879–2003, Boulder, Colorado: USA National Snow and Ice Data Center, 2008. 2008.

Wolff, C., Plessen, B., Dudashvilli, A. S., Breitenbach, S. F., Cheng, H., Edwards, L. R., and Strecker, M. R.: Precipitation evolution of Central Asia during the last 5000 years, The Holocene, 27, 142-154, https://doi.org/10.1177/0959683616652711, 2017.

Żarczyński, M., Tylmann, W., and Goslar, T.: Multiple varve chronologies for the last 2000 years from the sediments of Lake Żabińskie (northeastern Poland) – Comparison of strategies for varve counting and uncertainty estimations, Quaternary Geochronology, 47, 107-119, https://doi.org/10.1016/j.quageo.2018.06.001, 2018.

Zhou, A., Chen, F., Qiang, M., Yang, M., and Zhang, J.: The discovery of annually laminated sediments (varves) from shallow Sugan Lake in inland arid China and their paleoclimatic significance, Science in China Series D: Earth Sciences, 50, 1218-1224, https://doi.org/10.1007/s11430-007-0081-1, 2007.

Zolitschka, B., Francus, P., Ojala, A. E. K., and Schimmelmann, A.: Varves in lake sediments – a review, Quaternary Science Reviews, 117, 1-41, https://doi.org/10.1016/j.quascirev.2015.03.019, 2015.

https://doi.org/10.5194/gchron-2019-18
Preprint. Discussion started: 20 January 2020

Tables

Core ID	Latitude	Longitude	Depth (m)
CHAT12	40°36.370	75°14.020	20
SC17_1	40°36´756	75°14´481	15.05
SC17_2	40°36´587	75°15´138	17.25
SC17_3	40°36´315	75°14´577	18.25
SC17_4	40°39´124	75°19´891	5-10
SC17_5	40°36´363	75°14´079	19.5-20
SC17_6	40°36´213	75°13´939	19.2
SC17_7	40°36´147	75°14´062	18.5

Table 1: Coordinates of long and short cores.

https://doi.org/10.5194/gchron-2019-18
Preprint. Discussion started: 20 January 2020

Depth (cm)	LabID	^{14}C	Error	cal. years BP (2σ range)	cal a BP (midpoint + span)	material
0	Poz-109830	5050	40	5908-5664	5786±122	leaves
0	Poz-54280	330	30	308-473	391±83	recent aquatic plant
0	Poz-54281	2425	25	2354 - 2692	2523±169	recent aquatic plant
0	Poz-54279	225	30	-4 - 310	155±155	recent *Daphnia*
38.5	Poz-54282	755	35	660 - 735	697±36	aquatic plant
41.5	Poz-56609	1265	30	1088 - 1285	1187±98	bulk TOC
59.5	Poz-54283	955	30	798 - 964	881±83	aquatic plant
88	Poz-54286	1595	30	1410 - 1549	1480±69	aquatic plant
98	Poz-54284	1715	35	1552 - 1706	1629±77	aquatic plant
98.7	Poz-56614	1730	30	1564 - 1708	1636±72	aquatic plant
98.7	Poz-556592	2220	30	2152 - 2324	2238±86	bulk TOC
111	Poz-54287	1925	30	1817 - 1947	1882±65	*Daphnia* remain
115.5	Poz-54288	1960	30	1830 - 1989	1910±79	*Daphnia* remain
179.5	Poz-56596	4150	35	4572 - 4827	4700±128	bulk TOC
209.7	Poz-56610	4930	35	5597 - 5727	5662±65	bulk TOC
229.5	Poz-54289	5790	50	6415 - 6665	6540±125	*Daphnia* remain
252	Poz-56595	5840	40	6533 - 6747	6640±107	bulk TOC
255.7	Poz-54290	5880	35	6637 - 6785	6659±126	*Daphnia* remain
299.7	Poz-56593	6840	40	7591 - 7757	7674±83	bulk TOC
345	Poz-56594	7610	40	8025 - 8180	8103±78	bulk TOC
345	Poz-54292	7305	35	8350 - 8514	8432±82	bulk TOC
370.1	Poz-56613	8200	50	9015 - 9300	9158±143	bulk TOC
380.5	**Poz-63307**	**5360**	**40**	**6003 - 6277**	**6140±137**	**wood**
391.4	Poz-54294	8550	50	9465 - 9604	9535±70	*Daphnia* remain
391.7	Poz-54293	8710	50	9546 - 9887	9717±171	*Daphnia* remain
437.2	Poz-54296	9160	50	10230 -10487	10359±129	*Daphnia* remain
439.9	Poz-56611	9360	50	10427 - 10713	10570±143	bulk TOC
466	Poz-54297	9670	50	10789 - 11211	11000±212	*Daphnia* remain
469	Poz-54298	9690	50	10795 - 11226	11011±216	*Daphnia* remain
508	Poz-54299	10840	50	12681 - 12804	12743±62	*Ruppia maritima*
510	Poz-54300	11060	50	12790 - 13062	12926±136	bulk TOC
528	Poz-54301	12150	50	13831 - 14175	14003±172	bulk TOC
528	**Poz-54302**	**8890**	**50**	**9785 - 10191**	**9988±203**	**deciduous wood**
549.5	Poz-56591	12820	60	15105 - 15550	15328±223	bulk TOC
571	Poz-56608	13220	70	15660 - 16125	15893±233	bulk TOC
585	Poz-63308	14060	90	16759 - 17419	17089±330	*Ruppia maritima*
620.5	Poz56590	13190	70	15612- 16092	15852±240	bulk TOC

Table 2: ^{14}C dates (calibrated with OxCal 4.3, IntCal13).

https://doi.org/10.5194/gchron-2019-18
Preprint. Discussion started: 20 January 2020

Figures

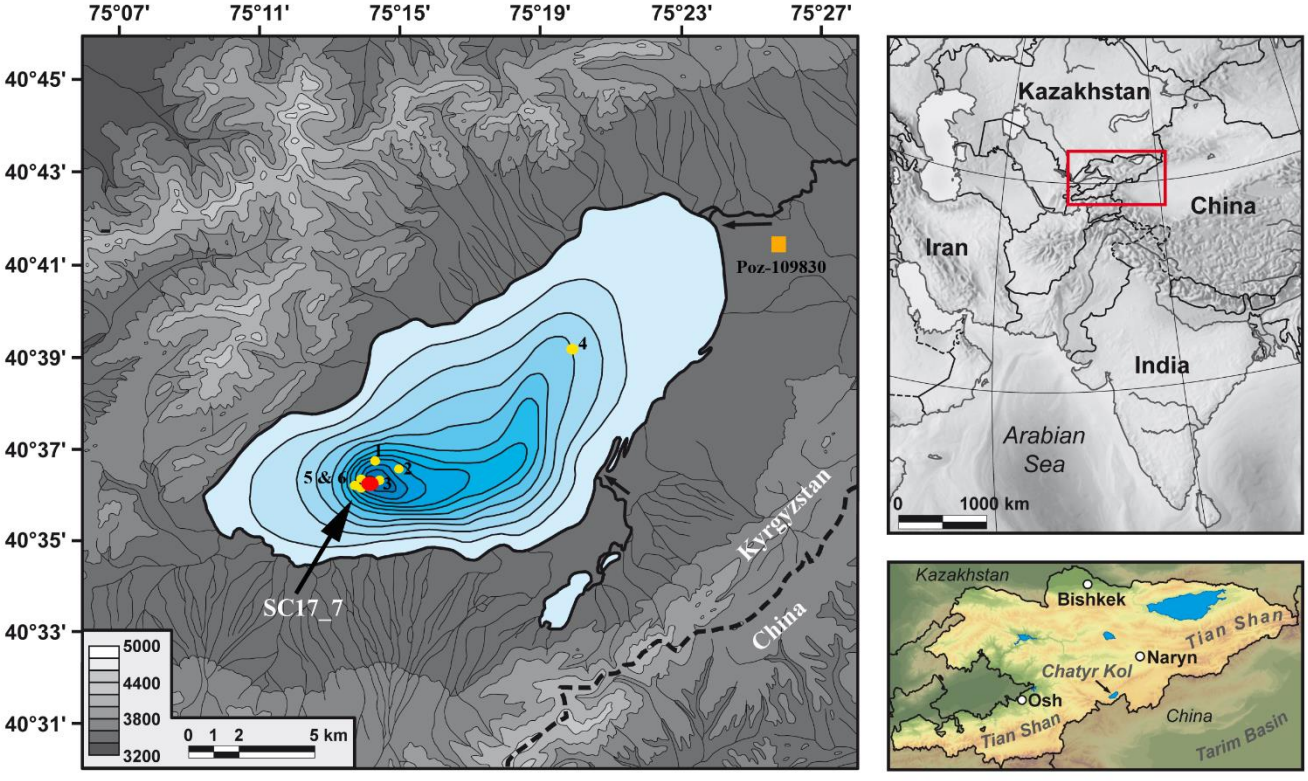

Figure 1: Location of Lake Chatyr Kul, the composite profile (red dot) and the gravity cores (yellow dots). The orange square marks the location of ^{14}C dated leaves (Poz-109830, Tab. 2) found in the top of a mid-Holocene-shoreline at ~3540 m a.s.l. The relief map of Kyrgyzstan relies on the CGIAR-CSI SRTM 90m (3 arcsec) digital elevation data (Version 4) of the NASA Shuttle Radar Topography Mission (Jarvis, 2008). The figure was modified from Lauterbach et al. (2014).

https://doi.org/10.5194/gchron-2019-18
Preprint. Discussion started: 20 January 2020

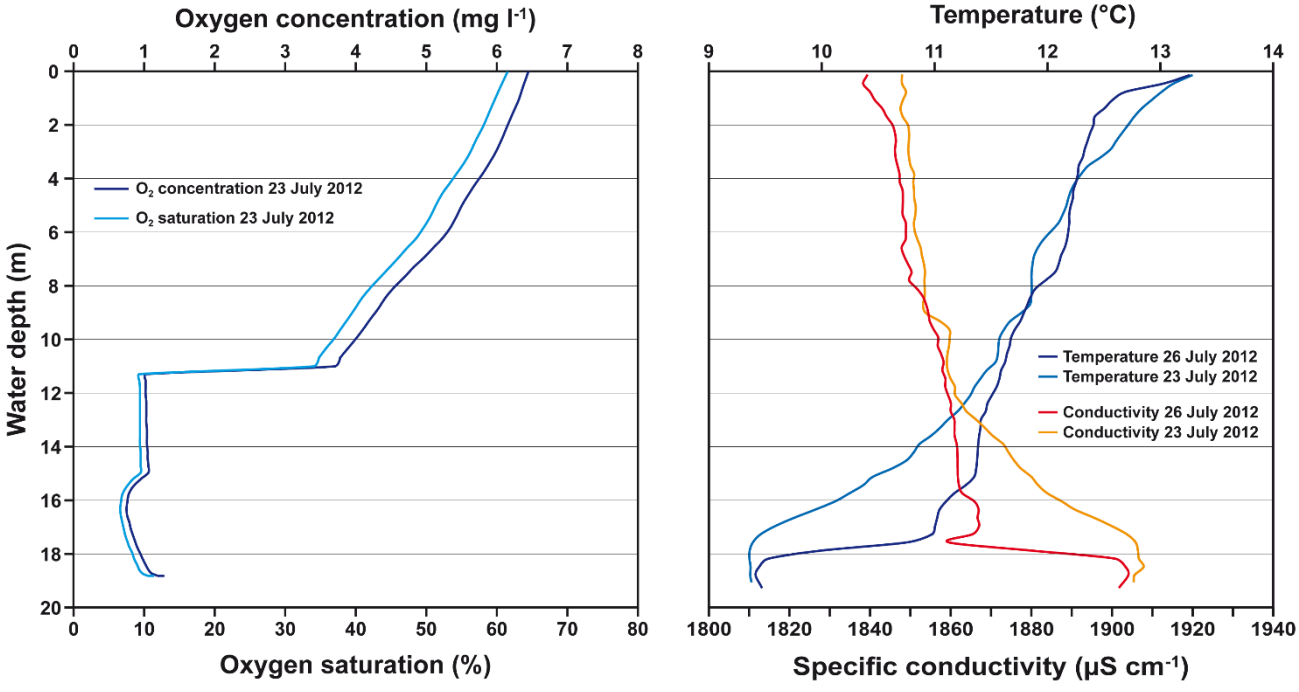

Figure 2: Oxygen concentration (YSI Pro 6600 V2), Temperature and specific conductivity measured with a CTD sensor during the field trip in 2012 at the core´s location (N 40°36.371´, E 75°14.006´).

https://doi.org/10.5194/gchron-2019-18
Preprint. Discussion started: 20 January 2020

Figure 3: The composite profile CHAT12 (dark grey: piston cores A5o, A5u, B3o, B1u and A4u). Additional gravity cores taken in 2017 (SC17_1 to SC17_7) were only partly used for thin section preparation and gamma spectrometry dating. The gravity cores cover approximately the upper first meter of the composite profile.

https://doi.org/10.5194/gchron-2019-18
Preprint. Discussion started: 20 January 2020

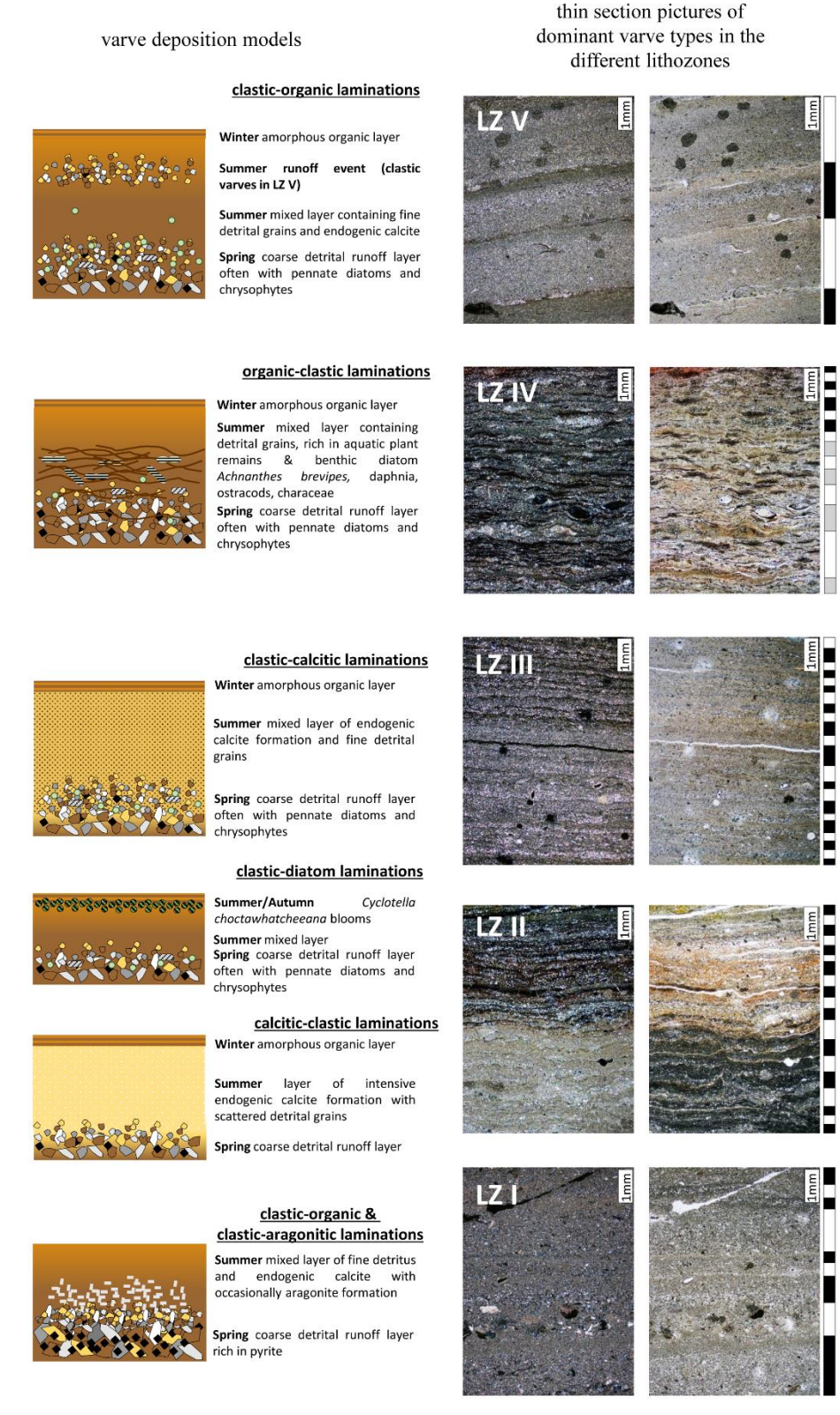

Figure 4: Thin section pictures of different lamination (varve) types in cross-polarized (left) and plane polarized (right) light of the different lithozones LZ I to LZ V. LZ I) Clastic-organic laminations; LZ II) Intercalation of clastic-organic, clastic-diatom and calcitic-clastic laminations; LZ III) Intercalation of clastic-calcitic, clastic-organic and clastic-diatom laminations (upper part); LZ IV) Organic-clastic laminations; LZ V) Clastic-organic laminations. Black/white/grey bars alongside the thin section pictures indicate one individual varve, but the reliability of grey bars (varves) is being generally lower due to high amounts of aquatic plant remains and low preservation. Process-related deposition Models of the observed lamination/varve types illustrate the seasonal depositional successions

https://doi.org/10.5194/gchron-2019-18
Preprint. Discussion started: 20 January 2020

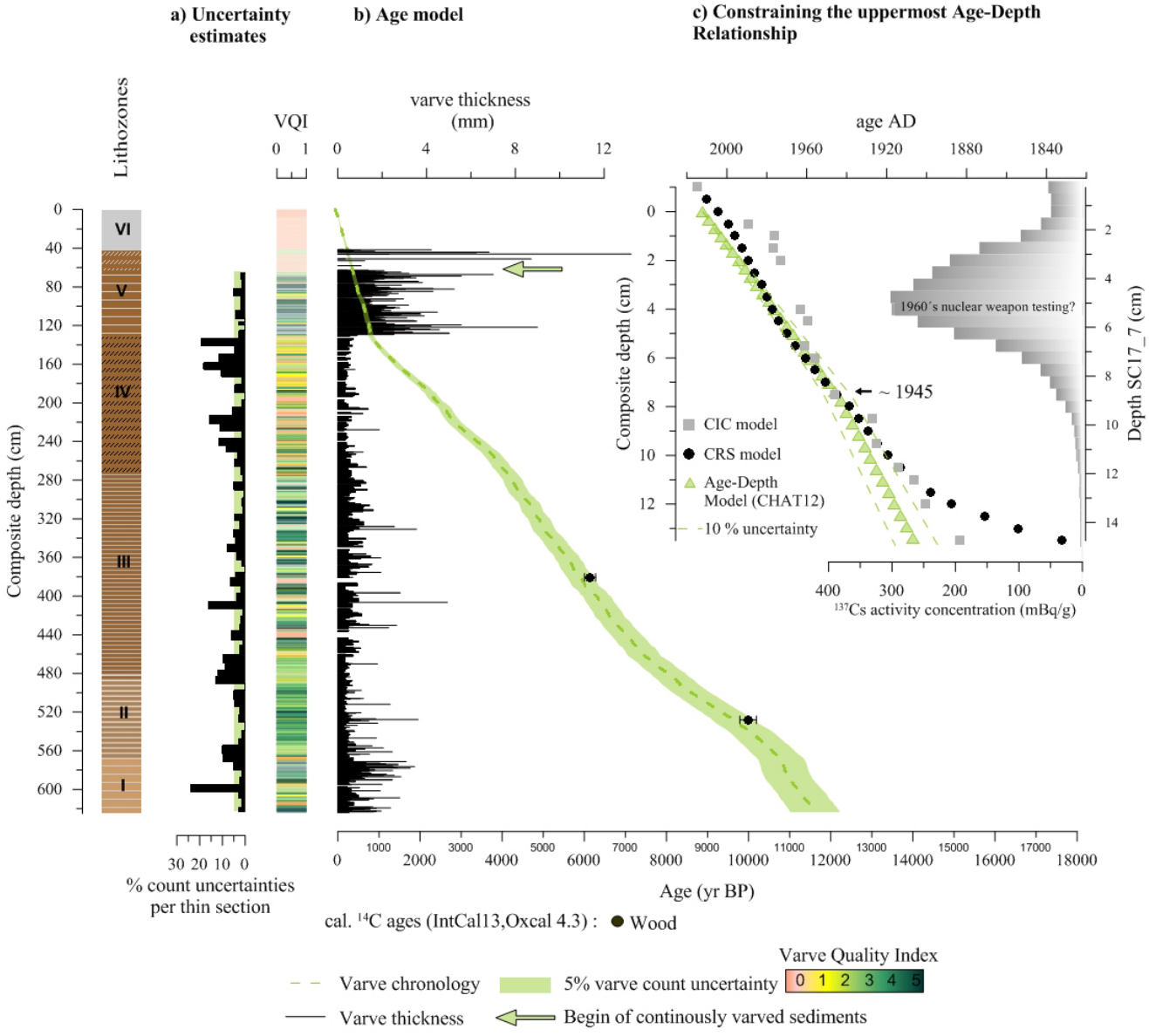

Figure 5: a) Varve counting uncertainty estimates (mean of 5% =green) and VQI distribution. b) Age model of the floating varve chronology (Chatvd19) from 63.0-623.5 cm depth with a basal age of 11619 ± 603 years BP (light green). The black line shows the measured varve thickness, black dots mark the distribution of calibrated AMS 14C ages (with 2σ uncertainty) of wood pieces (Tab.2). b) ^{210}Pb CIC (grey squares) and CRS (black dots) age models, ^{137}Cs activity concentration profile and constrained age model for the uppermost part of the composite profile (green triangles).

https://doi.org/10.5194/gchron-2019-18
Preprint. Discussion started: 20 January 2020

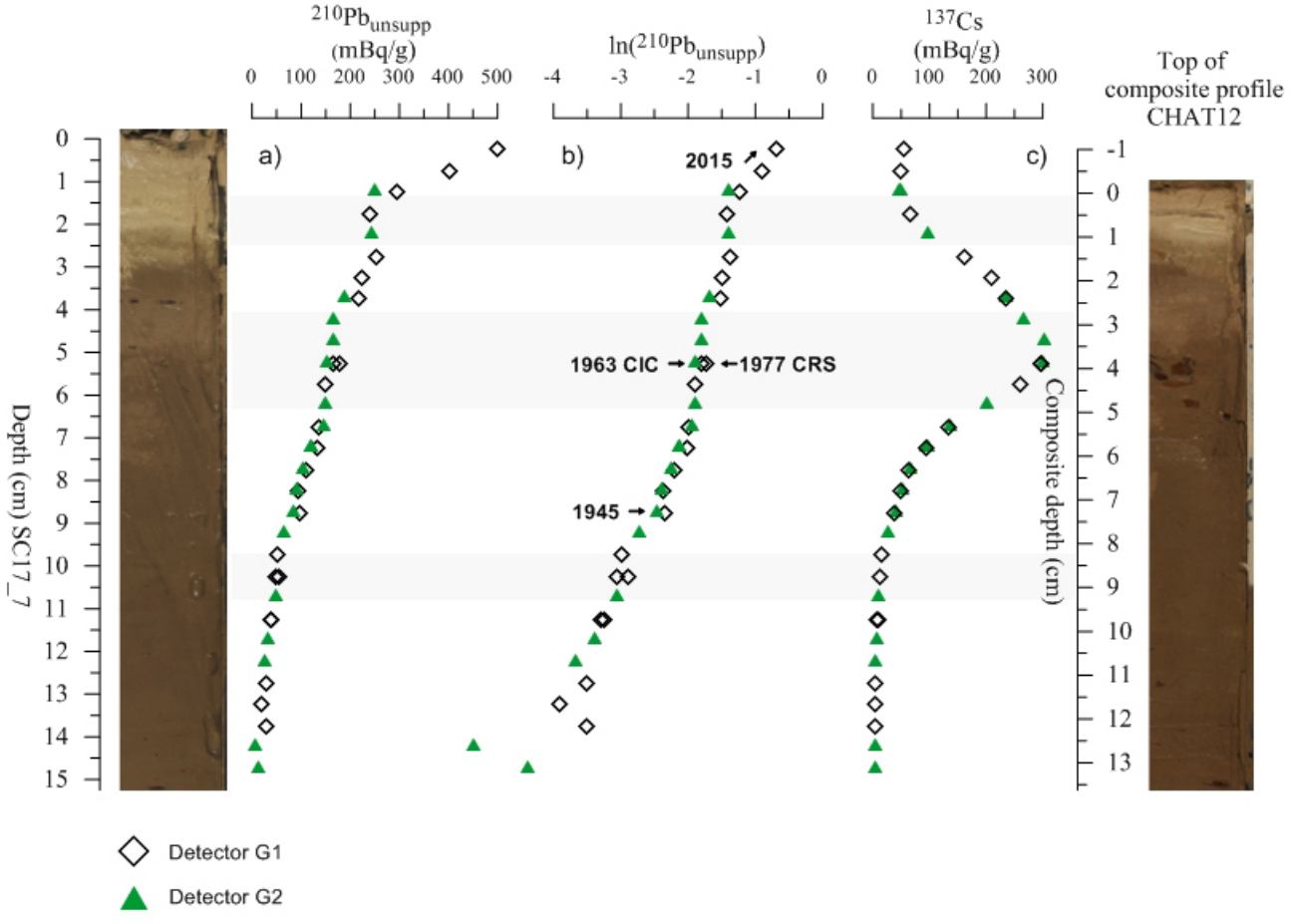

760 **Figure 6: Gamma spectrometry results of the gravity core SC17_7. Light grey intervals indicate uncorrelated sequences of the $\ln^{210}Pb_{unsupp}$ vs. depth profile which affected the CIC model calculations (Suppl. Fig.2, Suppl. Tab. 2, 3). Core pictures of the upper part of the composite profile CHAT12 (right) and the gravity core SC17_7 (left) illustrate the facies change to calcite-enriched sediments in the uppermost centimetres.**

765

770

https://doi.org/10.5194/gchron-2019-18
Preprint. Discussion started: 20 January 2020

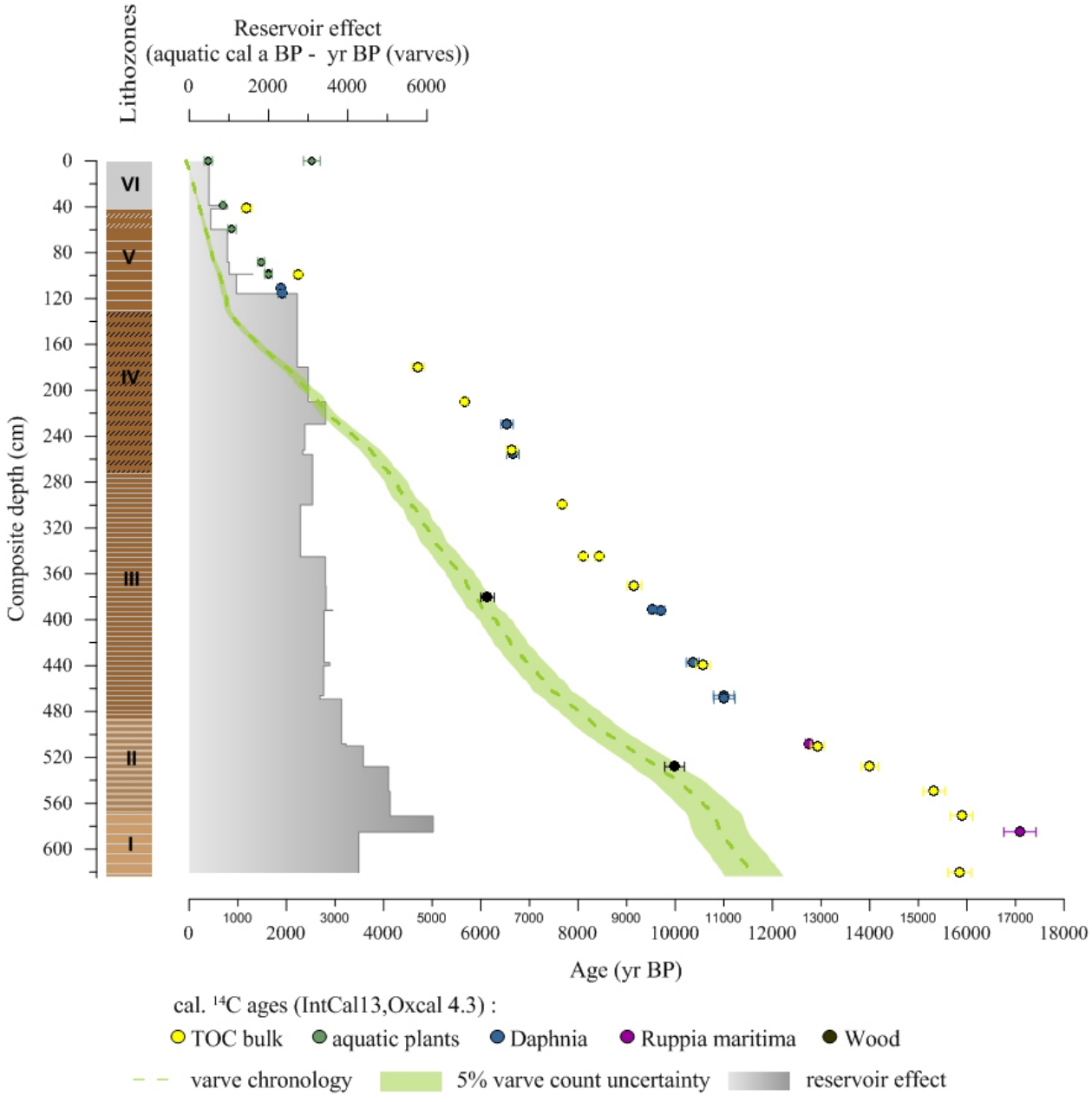

Figure 7: Radiocarbon reservoir effect (grey step plot). The reservoir effect was determined by the difference of aquatic cal. a BP (colored symbols) and varve ages (green). Floating varve chronology (green) and distribution of calibrated AMS ^{14}C ages (with 2σ uncertainty) of wood pieces, TOC bulk, aquatic plant remains, daphnia and *Ruppia maritima* remains (Tab.2).

https://doi.org/10.5194/gchron-2019-18
Preprint. Discussion started: 20 January 2020

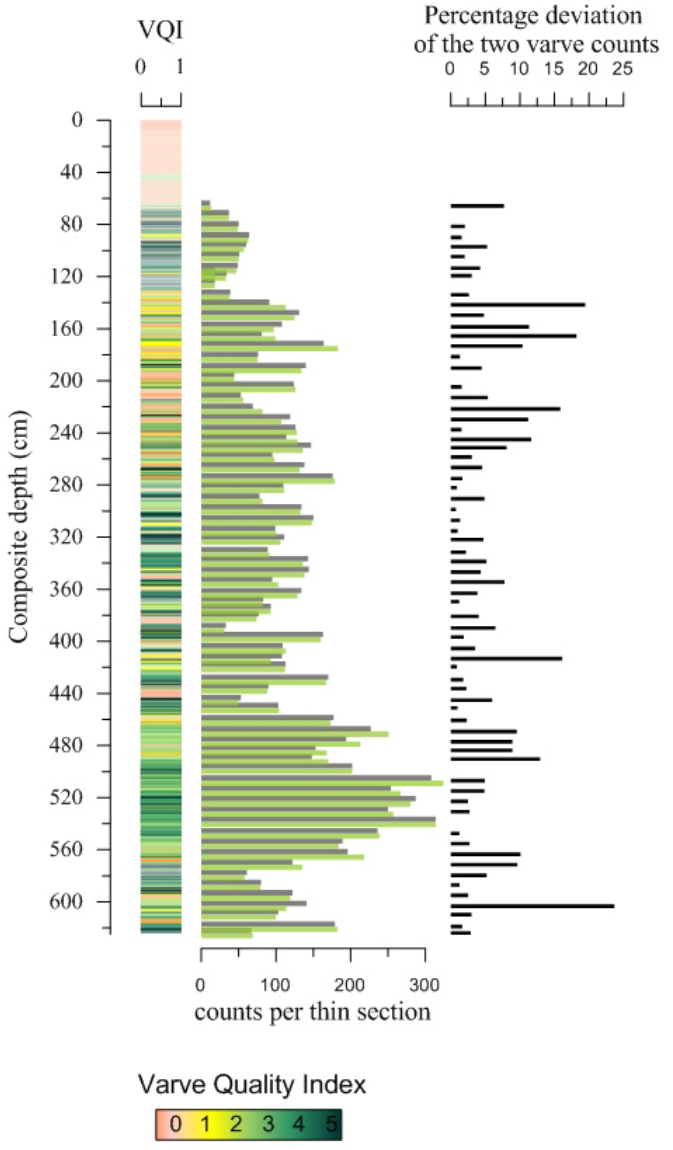

Figure 8: VQI, Counting differences for individual thin sections (green= 1st count, black = 2nd count, and their percentage deviation.

https://doi.org/10.5194/gchron-2019-18
Preprint. Discussion started: 20 January 2020

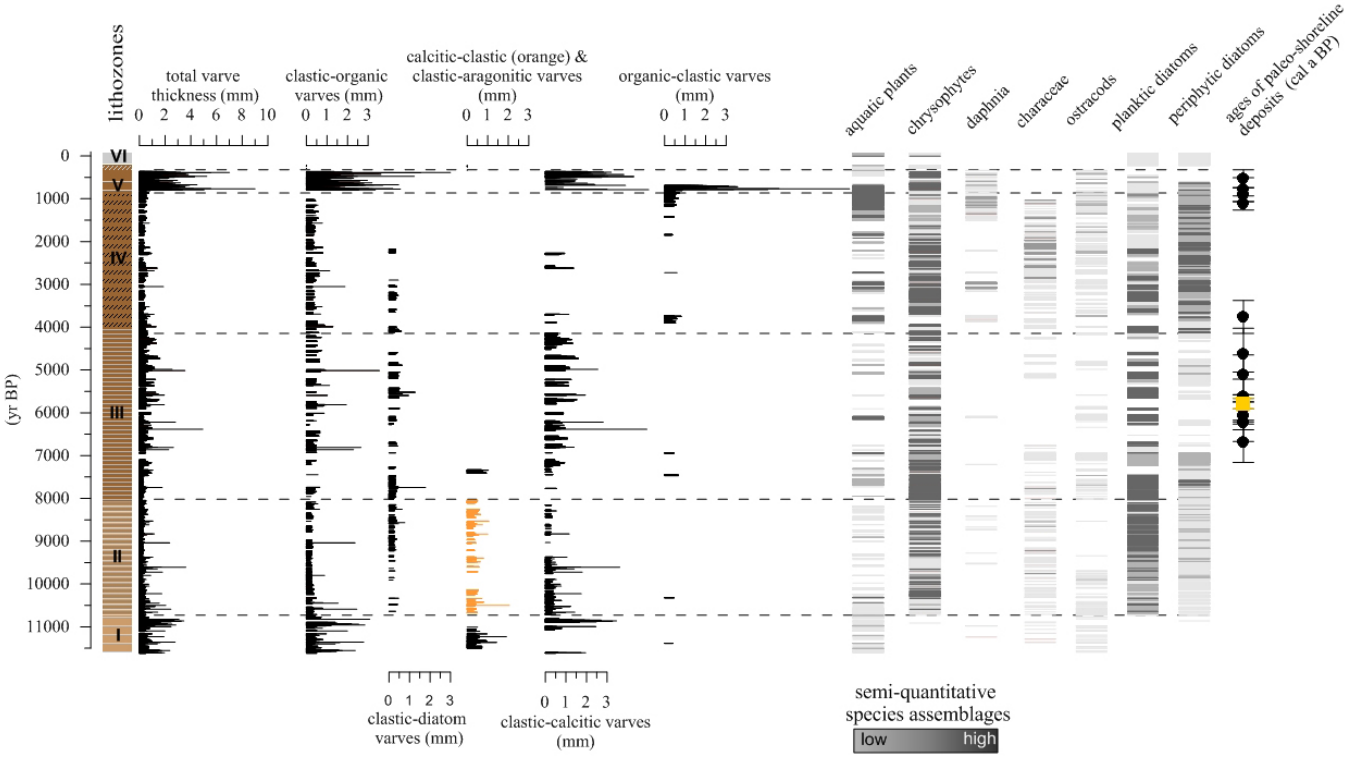

785 **Figure 9: a) Holocene seasonal deposition patterns, semi-quantitative species assemblages and calibrated 14C dates of paleo-shore deposits (black dots from Shnitnikov (1978), yellow square from own sample taken in 2017 (Table 2).**